Deep Tectono-Geodynamic Aspects of Development of the Nubian-Arabian Region and Its Relationship with Subsurface Structure

Lev Eppelbaum and Youri Katz

Abstract At present, a vital influence of regional tectono-geodynamical factors to environmental features is obvious. The Nubian-Arabian region contains such important geological-geophysical phenomena as (1) remnant collision of the ancient Neotethys Ocean, (2) wide development of the continental rifting zones with elements of triple junction, (3) a giant Ural-African geoid's step, (4) richest hydrocarbon reserves in the world, and (5) presence of the most ancient oceanic crust in the world (Kiama paleomagnetic hyperzone of inverse polarity). This region is also distinguished by several significant historical geological-geophysical events: (1) the Messinian crisis, (2) high seismicity, (3) active volcanism, (4) essential influence of sea level fluctuations and landscape changes to early hominid origin and evolution in Africa, and (5) uniqueness of the modern geological, geophysical and climatic regional factors. The significant influence of geological and geophysical factors on the environment is undoubted. However, we are only at the beginning of the study of this complex impact. For examination of the aforementioned problems, geophysical (satellite gravity, airborne magnetic, seismic, thermal, etc.) and geological (tectonic, geodynamical, structural, geomorphological, cyclic and event stratigraphy, paleobiogeographical, biochemical, etc.) methods were applied.

Keywords Tectonics · Geodynamics · Potential geophysical fields · Paleomagnetism · Complex physical-geological media · Relationship with environments

L. Eppelbaum (✉)
Porter School of the Environment and Earth Sciences, Faculty of Exact Sciences, Tel Aviv University, Tel Aviv, Israel

Azerbaijan State Oil and Industry University, Baku, Azerbaijan
e-mail: levap@tauex.tau.ac.il

Y. Katz
Steinhardt Museum of Natural History and National Research Center, Faculty of Life Sciences, Tel Aviv University, Tel Aviv, Israel

1 Introduction

The geological-geophysical background affecting all living system in our planet consists of many significant and not very significant environmental factors that are different in various regions of the Earth and their temporal changes. At the same time, the mutual influence of many of these factors is so complex that one of the factors considered insignificant suddenly turns out to be strongly nonlinear (e.g., Eppelbaum and Kardashov 2001) and its value can take on disastrous proportions.

The relation between the different geophysical (gravity, magnetic, thermal, radioactive, etc.) fields, geodynamic events (seismology), topographic pattern, and various environmental effects and animals' behavior is now accepted by international scientific community.

Among such effects can be noted: (1) relation between the Sun-Moon gravity-magnetic activity and number of tornadoes (Eppelbaum 2013; Eppelbaum and Isakov 2015), (2) correlation relation between the number of Sun's spots and mud volcano activity (Alizadeh et al. 2016), (3) relationship between the bird migration and Earth's magnetic field characteristics (Wiltschko and Wiltschko 2014; Gould 2017), (4) relationship between the bird migration and gravity field (Blaser et al. 2014), (5) animals' behavior before the seismological events (Logan 1977; Nikonov 1992; Sheldrake 2005), (6) thermal interrelation between coral reef and adjoining sea (Monismith et al. 2006), and (7) obviously, topographic pattern of that time that enabled to realize the human migration from Africa only through the territory of modern Israel (Hershkovitz et al. 2018). This listing may be enormously extended. However, it should be noted that research of this kind is mainly at the initial stage.

According to Khalilov (2011) data, the most part of human population in the prehistorical and historical periods has been tending to occupy the seismically dangerous regions. The author associated this phenomenon with heightened fertility of soils in these regions.

The Nubian-Arabian region discussed in this chapter has entangled geodynamic elements including high seismic activity and collision processes, active rift zones, ridiculous structural mosaics made up of the intricate block system of oceanic and continental crusts of different ages, as well as several largest gravity anomalies and intricate magnetic field pattern. This region is characterized by presence of the richest hydrocarbon reserves and an enormous number of other economic deposits. Examination of gravity (satellite derived) and magnetics (mainly airborne) data was employed to develop a few of novel maps indicating the vital properties of the deep structure of the region.

The area under study presents a giant region of the Near and Middle East and Eastern (and partially—Northern) Africa (see Fig. 1). Its regional geological-geophysical peculiarities are presented (e.g., Stacy et al. 1980; Ben-Avraham and Ginzburg 1990; Glennie et al. 1990; Said 1990; Johnson 1998; Khain 2001; Ben-Avraham et al. 2002; Davis and Slack 2002; Pollastro 2003; Alsharhan and Nairn 2004; Robertson 2004; Stern et al. 2004; Jimenez-Munt et al. 2006; Reilinger et al. 2006; Hansen et al. 2007; Bordenave 2008; Johnson and Kattan 2008; Johnson

Fig. 1 Areal map of the studied region (on the basis of Google Earth) with some regional tectonic setting

et al. 2008; Scotese 2009; Milesi et al. 2010; Stern and Johnson 2010; Motavalli-Anbaran et al. 2011; Nyblade 2011; Reilinger and McClusky 2011; Stampfli et al. 2013; Korostelev et al. 2014; Muluneh et al. 2014; Eppelbaum and Katz 2015a, b, c, 2015a, b, c; Tunini et al. 2015; Alizadeh et al. 2016; de la Vara et al. 2016; Globig et al. 2016; Eppelbaum et al. 2018, 2020).

Without hesitation, regional tectonic-geophysical fragmentation will help scientists of different specialties to understand more precisely many biological and environmental phenomena of the region.

2 Data Analysis

As the main sources for regional fragmentation were utilized, the satellite gravity data (retracked to marine and land surfaces; sources of the data are noted in Sandwell and Smith 2009; Sandwell et al. 2013) and numerous examples of these data examinations are shown in Eppelbaum and Katz (2011, 2015a, b, c), Gaina et al. (2013), Klokočník et al. (2014), Eppelbaum and Katz (2017a, b, c), and Eppelbaum et al. (2018, 2020). Sources of the observed airborne (mainly) magnetic data were described in Maus et al. (2007). Besides the aforementioned data, seismic (Yakobson 1997; Krasheninnikov et al. 2005; Hansen et al. 2007; Pasyanos and Nyblade 2007; Park et al. 2008; Bastow et al. 2011; Nyblade 2011; Tunini et al. 2015), seismological (Camelbeeck and Iranga 1996; Davis and Slack 2002; Jimenez-Munt et al. 2006; Eppelbaum and Katz 2012b; Korostelev et al. 2014), GPS (McLusky et al. 2000; Wdowinski et al. 2004; Reilinger et al. 2006; Stamps et al. 2014), magnetic (Ben-Avraham et al. 2002; Stern and Johnson 2010; Eppelbaum 2015), paleomagnetic (Eppelbaum et al. 2014; Eppelbaum 2015; Eppelbaum and Katz 2014, 2015c, 2017a, b, c), and thermal (Cermak 1993; Pollack et al. 1993; Artemieva et al. 2006; Verzhbitsky 1996; Tainton et al. 1999; Eppelbaum and Pilchin 2006; Tunini et al. 2015; Globig et al. 2016) data were analyzed.

2.1 Brief Analysis of the Terrain Relief Field

A relationship between the deep geodynamics and terrain relief is widely discussed in literature (e.g., Khesin et al. 1996; Braun 2010; Cloetingh and Willet 2013). Application of different statistical-probabilistic procedures to terrain relief data is considered in detail in Khesin et al. (1996) and Eppelbaum and Khesin (2012). Examination of the topography field sometimes contains more information than geophysical field analysis especially in the context of studying different environmental problems. Figure 2 displays topography/bathymetry map of the studied region. Even the simple visual analysis indicates the complex topography within Alpine-Himalayan orogenic belt in the eastern part of the Mesozoic terrane belt.
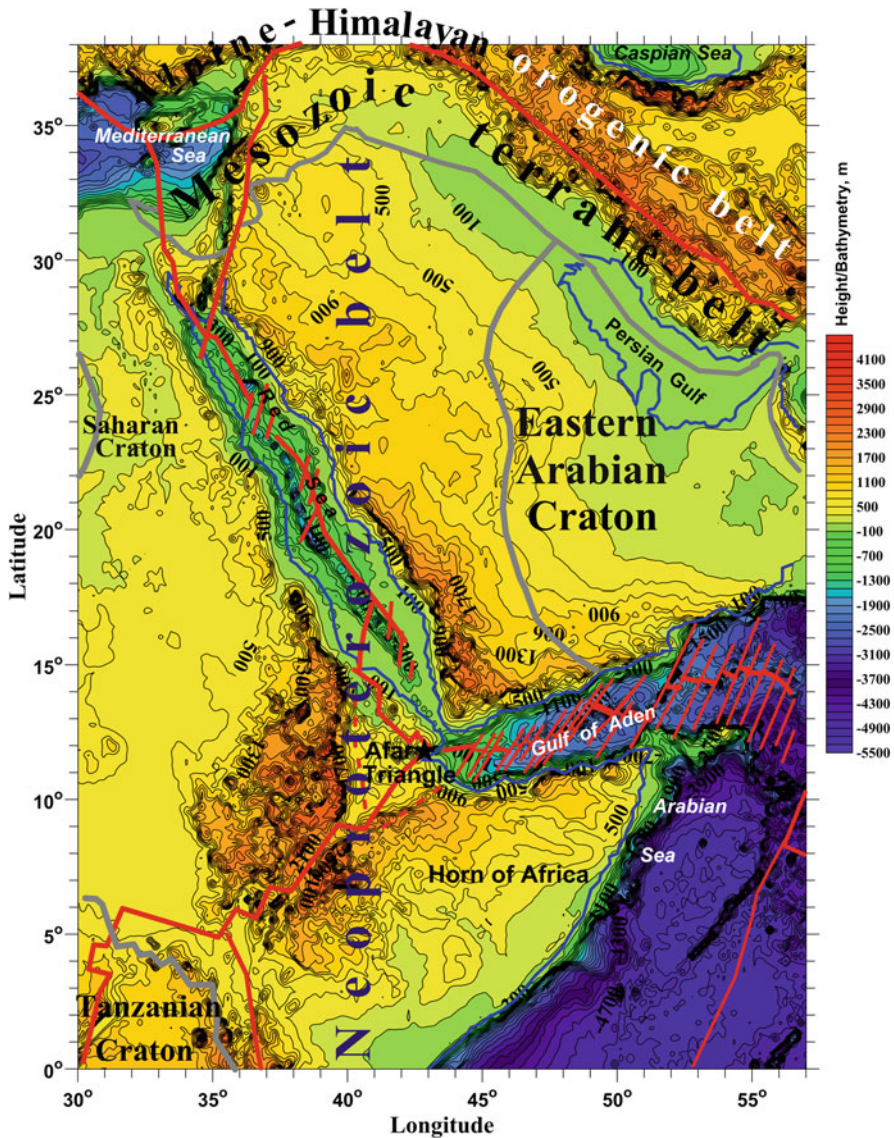
Fig. 2 Topography map of the studied region with tectonic setting. Symbol "filled star" designates location of triangle junction. Red lines indicate fault systems, gray lines show boundaries of cratons and tectonic belts, and blue lines show boundaries between the land and seas (ocean)

Complex terrain relief is observed in the southern part of the Neoproterozoic belt. A smoothed relief characterizes eastern Arabian and Saharan cratons and surrounding areas. The Red Sea and Gulf of Aden are presented by linear negative topographic forms, whereas within the Arabian Sea, the deepest bathymetry (about −5000 m) is

observed. A reflection of the tectonic-geodynamical effects in the terrain relief can be clearly seen in the next figures where gravity and magnetic maps and their transformants and paleomagnetic and seismological and some integrated geophysical-geological maps are presented.

2.2   Analysis of the Satellite-Derived Gravity Data

Previous conventional gravity observations (airborne and shipborne) were performed as single profiles or separate areal observations, with different precision of gravity field observation and different processing schemes. Besides this, the furthermost part of the accomplished measurements is estimated by the gravity data computation error of >2–3 mGal (1 mGal = 10^{-5} m/s^2) (sometimes even as high as 5 mGal).

We utilized the gravity data from the World Gravity DataBase as retracked from different satellite missions (e.g., Sandwell and Smith 2009; Andersen et al. 2009). These observations are realized with the global regular 1-min grids (Sandwell and Smith 2009), and the computation error was estimated as ~1–1.1 mGal (Sandwell et al. 2013). It is essential that in the satellite-derived data were reduced the effects of ruggedness and inaccessibility (Eppelbaum and Katz 2017a). Furthermore, the satellite gravity data employment allows to avoid appearing some fictitious anomalies produced by the combination of different scale surface gravity surveys (Braitenberg and Ebbing 2009).

The discussions concerning the kind of gravity satellite data retracked to marine (land) surface are not completed till the present. Nevertheless, many scientists believe that this gravity in the marine (ocean) areas can be supposed to be close to "free air" reduction (or "free air anomalies" = $\Delta g_{\text{f.a.}}$) (Sandwell et al. 2013; Eppelbaum and Katz 2017a).

The more complicated situation is detected in the land areas, where mountain belts can significantly affect $\Delta g_{\text{f.a.}}$ values. However, from our experience (Eppelbaum and Katz 2012b, 2015a, b, 2017a, b, c; Eppelbaum 2015, 2017a, b; Eppelbaum et al. 2018), it follows that for regional tectonic-geodynamical analysis of large areas (the studied region covers the area more than 1.3×10^7 km^2), where we analyze gravity anomalies from large depths, the satellite gravity data retracked to land surface can be examined without any additional corrections (reductions).

The compiled gravity map based on more than 4×10^6 satellite observations retracked to Earth's surface (Fig. 3) designates an intricate pattern of gravity field in the studied region and the key geotectonic features. Inspection of the gravity field pattern displayed in Fig. 3 recognizes two main classes of significant geotectonic units: (1) stable segments of continental and oceanic crust and (2) mobile geotectonic belts. The first type (stable zones) is characterized by the homogeneous property of the gravity field behavior (see, e.g., the Eastern Arabian Craton in Figs. 1 and 3), while the second type (mobile belts) is presented by mosaic and variable arrangement of gravity field (specifically, active rift zones). Examination of Fig. 3 proposes
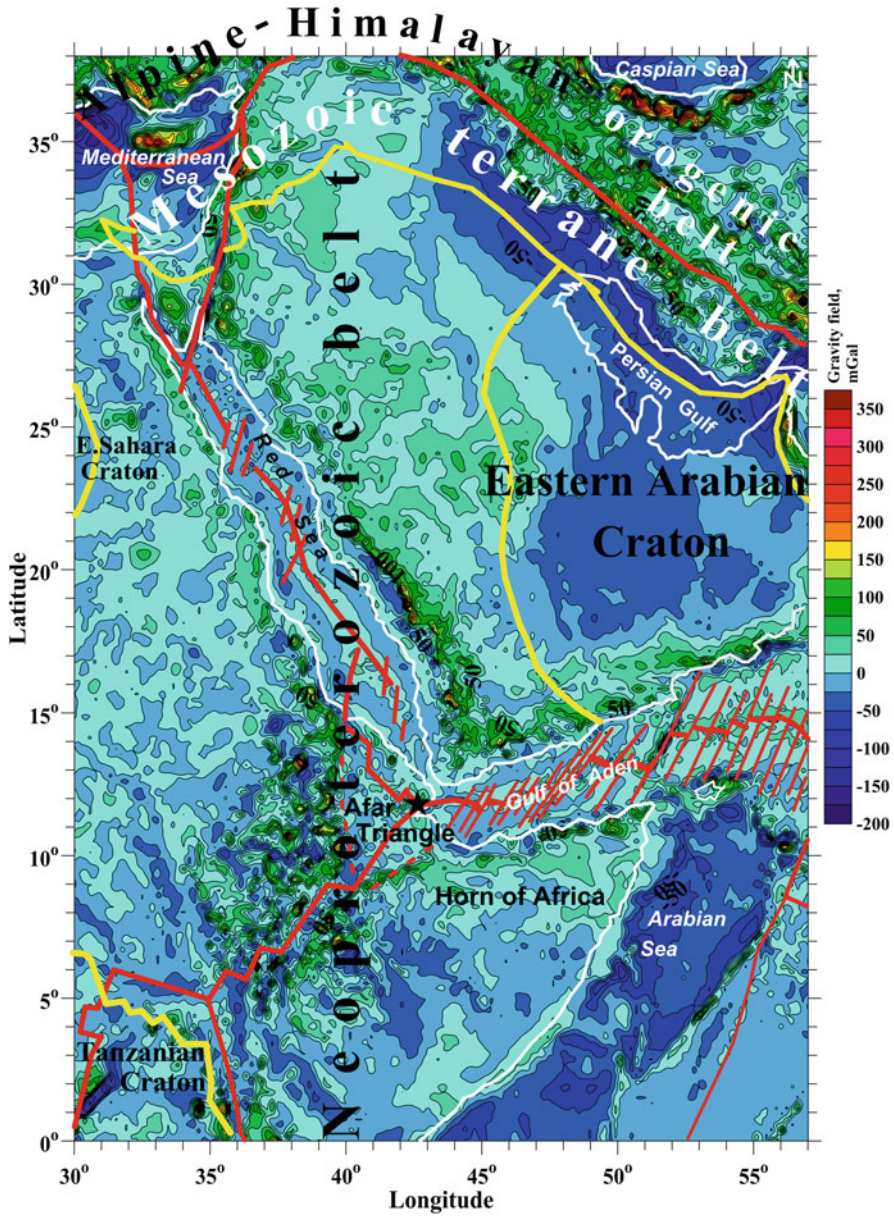
Fig. 3 Satellite-derived gravity map retracked to the Earth's surface and accompanied by general tectonic features. Red lines indicate fault systems, yellow lines show boundaries of cratons and tectonic belts, and white lines show boundaries between the land and seas (ocean)

that the Neoproterozoic belt and Mesozoic terrane belt significantly differ in the gravity field "portrait" from the "youngest" mobile tectonic structures (active rift systems of the Red Sea—East Africa and the Alpine-Himalayan orogenic belt).

Entropy map computation from the satellite gravity data was before effectively realized out in the Eastern Mediterranean (e.g., Eppelbaum and Katz 2015b). Applying the moving window of adaptive shape enabled to compute the intricate entropy map in conditions of enormous superimposed gravity anomalies of different order. Application of the aforementioned methodology for the satellite-derived gravity data for the region under study indicates significant deep tectono-structural elements of the region (Fig. 4). Intricate pattern of the entropy field generates a transfer zone between the Somalian and Indian plates (this sector indicates high-intensive mosaic field) in the SE part of the region. This map unmistakably displays position of the Mesozoic terrane belt and certain transition fragment from the Victorian Plate to the Tanzanian Plate. Some preliminary results demonstrate that the computed entropy map has some relationship with the thermal flow distribution in the region (Eppelbaum and Katz 2017a).

Employment of the statistical multidimensional analysis (SMDA) is carried out with application of semiautomatic sliding frame of adaptive form (rectangular or inclined) that enables to compute the anomalous effects from the geological objects with different geometric parameters along the strike; normal background pattern was automatically recognized (Fig. 5). SMDA implementation to the satellite gravity data allowed to outline geodynamical features of the region under study (for instance, active rift zones between the Nubian, Somalian, and Arabian plates and collision segment at the margin between the Arabian and Eurasian plates) and to reveal some essential tectonic features of the Earth's crust (Fig. 5). In the SMDA map, the oceanic crust zones are clearly traced: the Gulf of Aden, the eastern part of the Somalian Plate, and the Easternmost Mediterranean. This map also indicates the East African and Arabian active rift zones as well as collision junction between the Arabian and Eurasian plates.

Map of the gravity coherence amplitude (Fig. 6) was computed for the Eastern-most Mediterranean region. Basically, this method consists of dividing the area under study into subdomains with the different degrees of coherency (for instance, Alperovich et al. 2013). Absence of coherence (or low values of coherence) indicates a homogeneous medium. This map visibly displays some gradient zones (boundary between the oceanic and continental crust, high-amplitude Cyprus gravity anomaly, Dead Sea Transform, Mediterranean Ridge, Northern Western basin, etc.).

2.3 Analysis of the Airborne (Mainly) Magnetic Data

The magnetic data were obtained from the World Digital Magnetic Anomaly Map (WDMAM) collection compiled by the US Geological Survey (http://earthexplorer. usgs.gov/). The WDMAM project aimed to integrate all available airborne, near-surface, and satellite magnetic anomaly data into a global map database with the
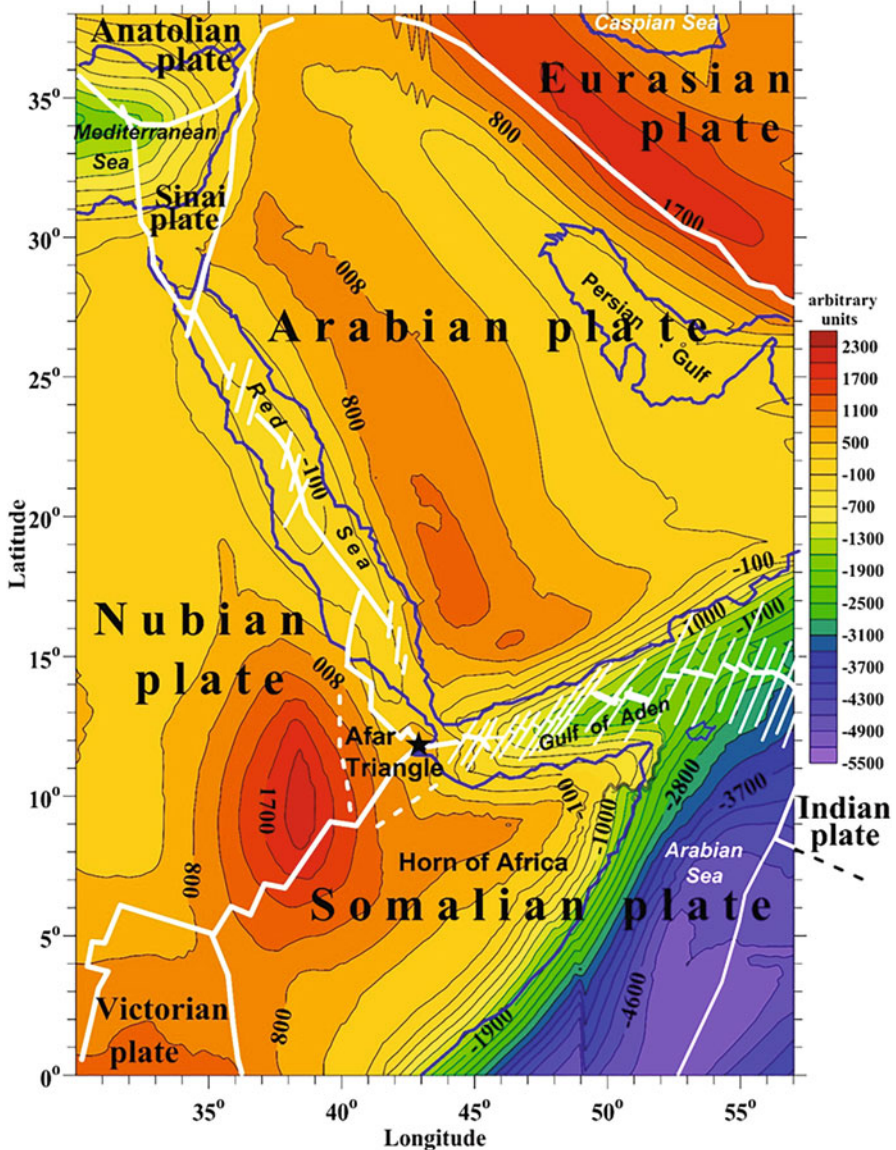
Fig. 4 Entropy map transformed from the satellite gravity map and accompanied by main tectonic features. Red lines indicate fault systems, yellow lines show boundaries of cratons and tectonic belts, and white lines show boundaries between the land and seas (ocean)

averaged level of 5 km over the mean sea level (msl). The compiled magnetic map accompanied by the regional tectonic setting is shown in Fig. 7. This map displays a complex mosaic behavior of magnetic anomalies with some homogeneous areas in

Fig. 5 Map of satellite-derived gravity field transformed by the use of statistical multidimensional analysis with location of the main plate tectonic units. White lines indicate fault systems; blue lines show boundaries between the land and seas (ocean)

(and in the vicinity) of the Eastern Arabian Craton and in the northern part of the Neoproterozoic belt. It should be noted a definite similarity between the magnetic field map (Fig. 7) and the satellite-derived gravity map (Fig. 2). In the averaged magnetic map (Fig. 8), numerous small anomalies are eliminated, and generally, it is
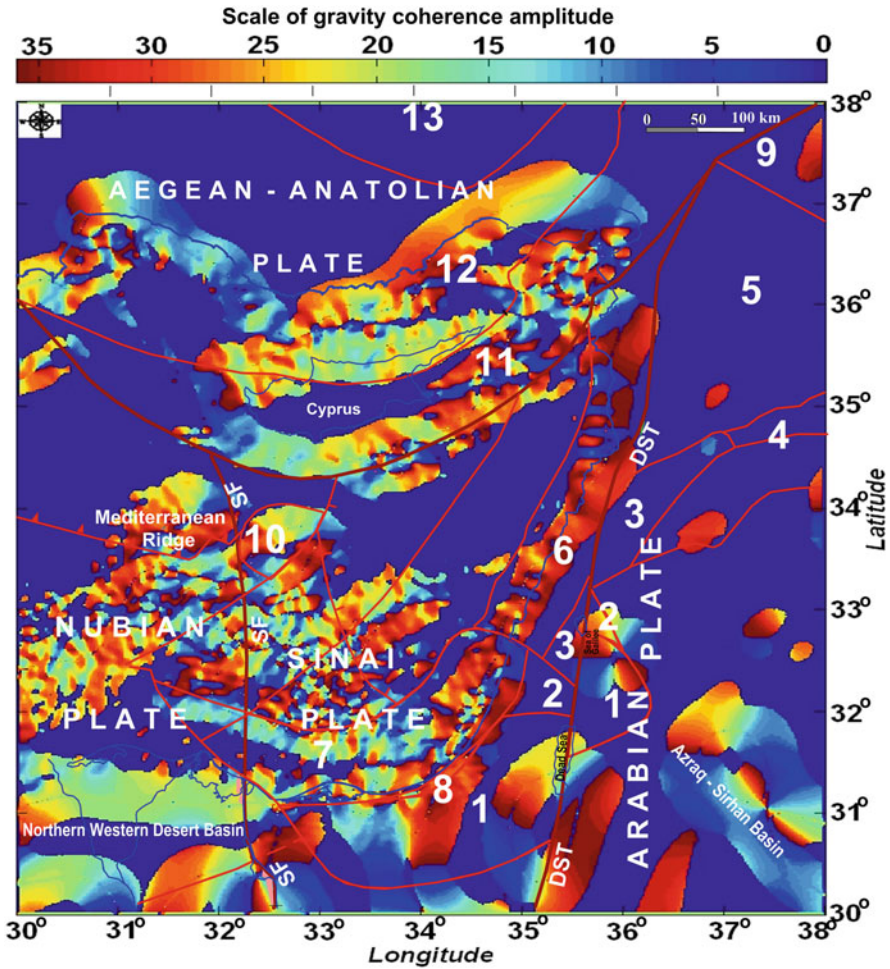
Fig. 6 Map of the satellite-derived gravity coherence amplitude. Position of tectonic terranes (large white numbers): (1) Negev, (2) Judea-Samaria, (3) Anti-Lebanon, (4) Palmyride, (5) Aleppo, (6) Galilee-Lebanon, (7) Pleshet, (8) Heletz, (9) Abdelaziz, (10) Eratosthenes, (11) South Taurides, (12) Taurus, (13) Anatolides; *SF* Sinai Fault, *DST* Dead Sea Transform. A scale on the top of this map shows coherence intensity (after Eppelbaum (2017a), with modifications)

a more readable one. This map shows a good correlation with the regional tectonic setting. A rich magnetic pattern presented in the gradient operator map (Fig. 9) closely agreed with the tectonic features. It is interesting to note that the central part of the Eastern Arabian Craton and northern continuation of the Neoproterozoic belt are practically free from the anomalous magnetic pattern. On the whole, analysis of the magnetic maps of this region (Figs. 7 and 8) indicates a significant difference between the marine and oceanic basins bordering the Arabian Plate (Mediterranean,
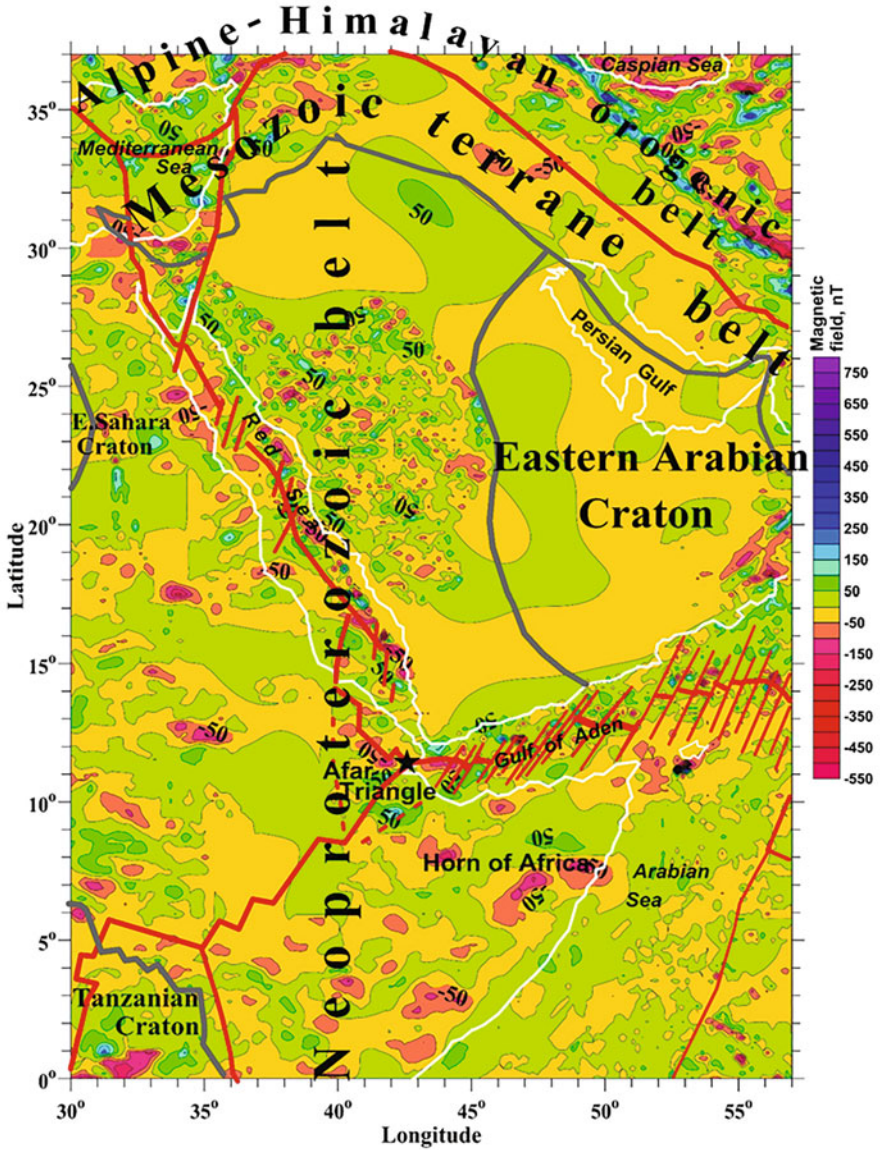
Fig. 7 Magnetic map of the studied region supported by the regional tectonic setting. Red lines indicate fault systems, gray lines show boundaries of cratons and tectonic belts, and white lines show boundaries between the land and seas (ocean)

Arabian Sea and Gulf of Aden basins) from the continental plates and mobile belts. Dominating here directly magnetized anomalies are characteristics of the basaltic crust (mainly of the Mesozoic and Cenozoic age), which composes its base. This is especially clearly illustrated by transition of the continental crust of the Horn of
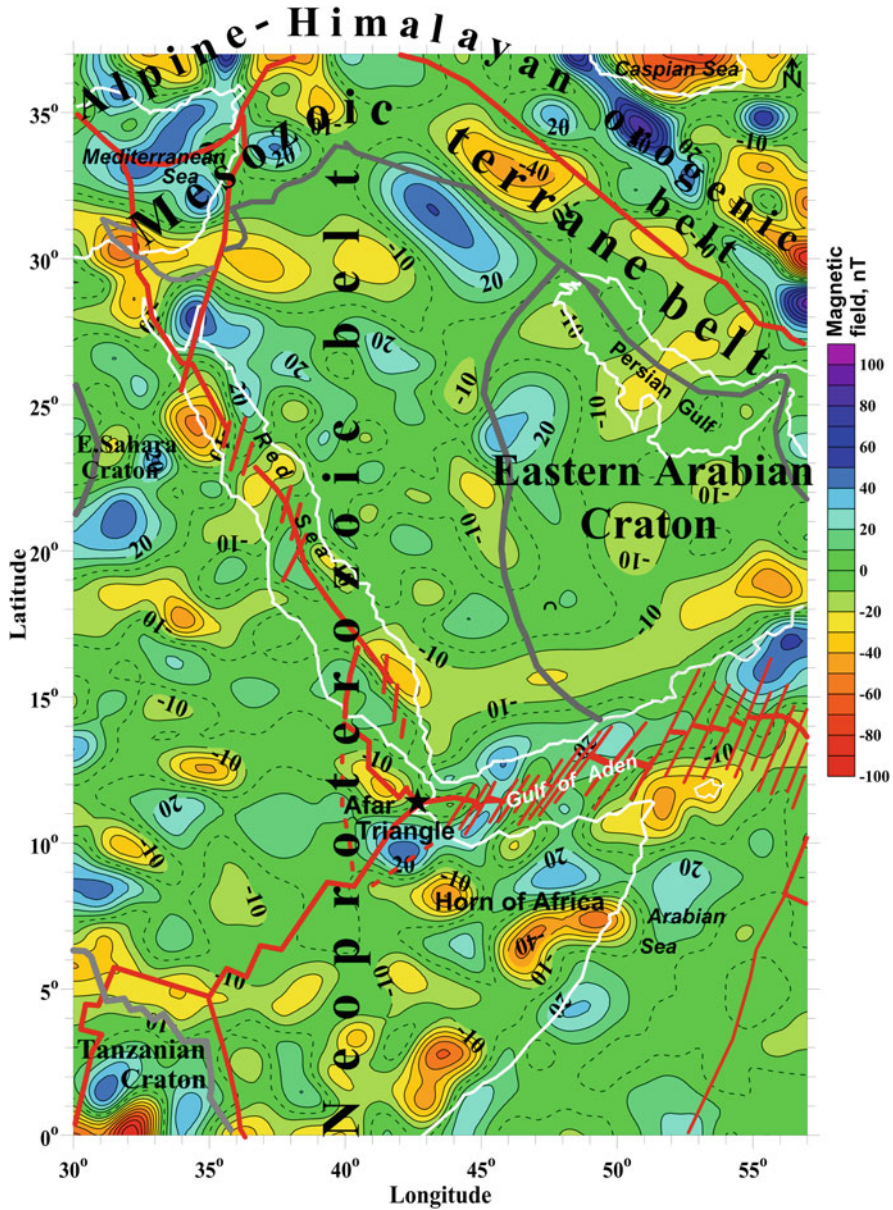
Fig. 8 Magnetic field map averaged by nine nodes. The designations are the same as in Fig. 7

Africa to the oceanic crust of the Arabian Sea (Figs. 7 and 8). A similar trend is also developed in the Eastern Mediterranean, where the common imaging is somewhat complicated by young magmatism superimposed on the continental crust stretching from the Red Sea to the Carpathians (Eppelbaum et al. 2020). Detailed examination
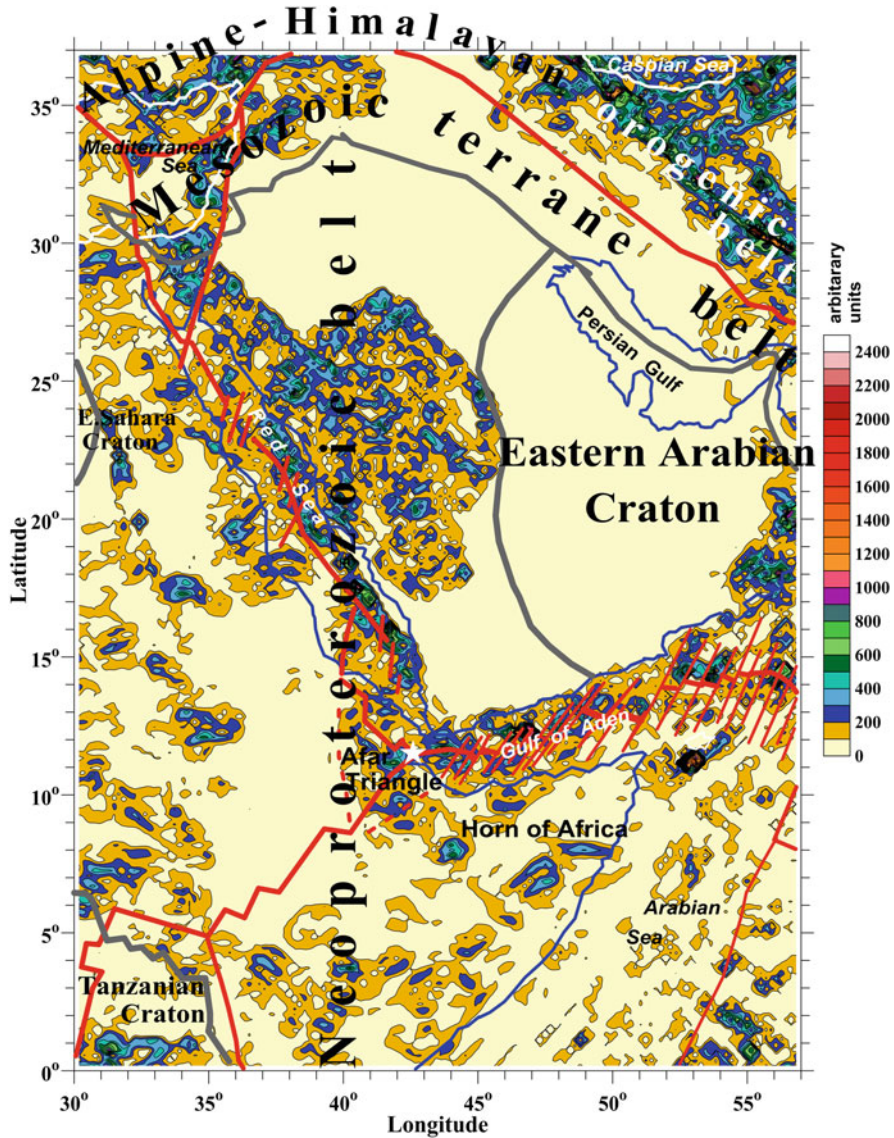
Fig. 9 Magnetic field processed by the gradient operator. Red lines indicate fault systems, gray lines show boundaries of cratons and tectonic belts, and blue lines show boundaries between the land and seas (ocean) (Easternmost Mediterranean and Caspian seas' boundaries are shown by white lines)

of magnetic anomalies and their relationship with the gravity and thermal data is subject of a separate study.

As was shown in Eppelbaum et al. (2014) and Eppelbaum and Katz (2015a), the Mesozoic terrane belt (including blocks of continental and ocean crust with the
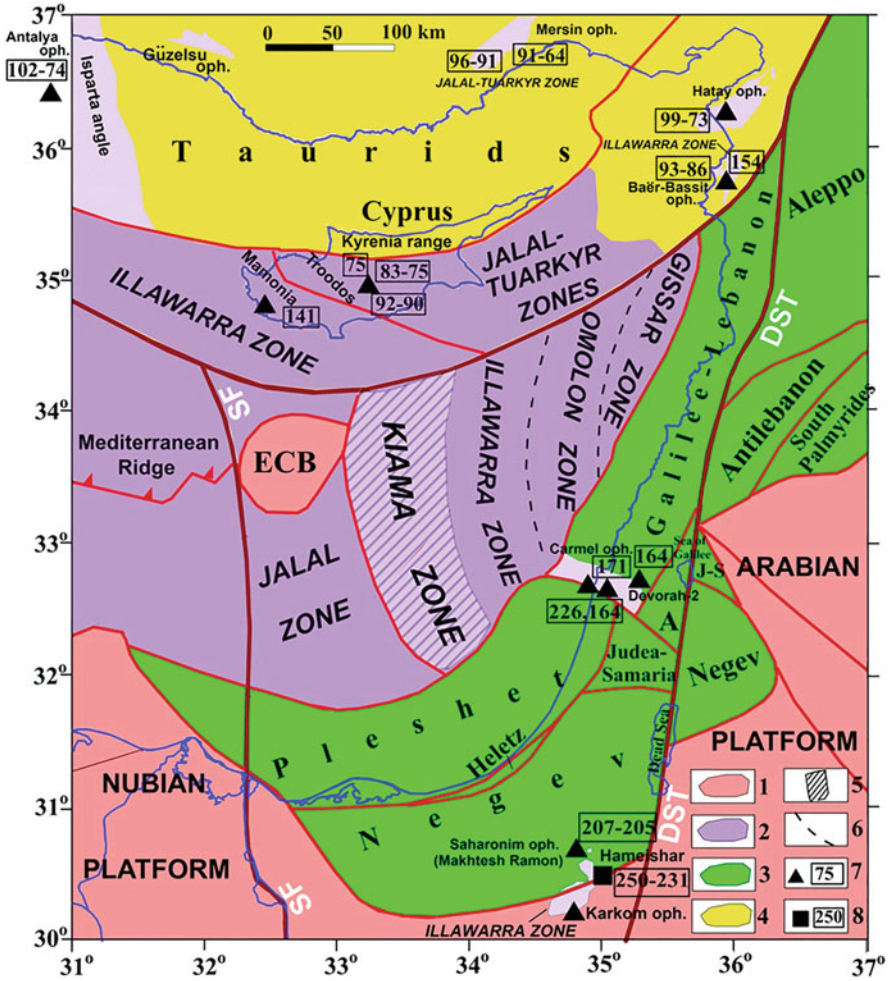
Fig. 10 Paleomagnetic zones in oceanic crust of the Eastern Mediterranean (after Eppelbaum and Katz 2014, 2015b, 2017b, 2020). Tectonic setting: (1) Precambrian crust, (2) Mesozoic oceanic crust, (3) Mesozoic terranes, (4) Alpine tectonic belt, (5) contour of the Kiama paleomagnetic hyperzone, (6) proposed boundaries between the paleomagnetic hyperzones, (7) magmatic rocks of obduction zones and their age, (8) magmatic rocks of subduction zones and their age. *SF* Sinai Fault, *DST* Dead Sea Transform, *ECB* Eratosthenes Continental Block

tectonic units of Kiama, Illawarra, and some other paleomagnetic zones) (Fig. 10) was moved anticlockwise (about 120 Ma) along transform faults from the region of the present Eastern Persian Gulf. These constructions (comprehensive 3D magnetic field modeling has been supported by 3D gravity field modeling and seismic data analysis) are based on geochronological and tectono-structural data from Early-Late Permian traps (Negev and Heletz terranes), Permian basalts of Hameishar, Triassic Saharonim basalts of Makhtesh Ramon, and Triassic-Jurassic spilites, keratophyres,

basalts, and gabbroids of Mt. Carmel. The discrepancy between the terrane belt and the Gondwana foreland, oceanic crust, and terrane belt indicates the allochthonous nature of the Eastern Mediterranean (Eppelbaum and Katz 2015a; Eppelbaum et al. 2019). The integrated tectono-geophysical and paleogeographical specifics of deep zonation call for a reevaluation of regional criteria for oil and gas prospecting (first of all, for the Eastern Mediterranean).

2.4   Brief Analysis of Thermal Data

It should be noted that the Nubian-Arabian region is characterized by complex pattern of thermal flow (e.g., Martinez and Cochran 1989; Cermak and Rybach 1991; Pollack et al. 1993; Artemieva 2006; Artemieva et al. 2006; Verzhbitsky 1996; Lucazeau et al. 2009; Förster et al. 2010; Rolandone et al. 2013). Artemieva et al. (2006) associate some large thermal anomalies in the northern part of the region with differences of the thicknesses of the transition zone between purely conductive and purely convective heat transfer.

The thermal flow data observed in the Easternmost Mediterranean indicate sufficiently low values, from 11.5 up to 35 mW/m^2 (Erickson et al. 1977; Eckstein 1978; Cermak 1993; Elgabry et al. 2013; Eppelbaum and Katz 2015a), that in accordance with the analysis of Sclater et al. (1980), testify to the most ancient age of the oceanic Earth's crust. The minimal value of the thermal flow (11.5 mW/m^2) is observed in the marginal northern part of the reversely magnetized Kiama hyperzone (it corresponds possibly to the oldest block of the oceanic Earth's crust subducted upon the Aegean-Anatolian Plate). If we calculate the effect of sedimentation velocity (assumed at 18 cm/1000 years), the thermal values will increase only by about 15% and will be several times less than in the Western and Central Mediterranean. Eppelbaum and Pilchin (2006) firstly composed the first map of the Curie discontinuity of Israel (supported by a first map of the Moho discontinuity for the Eastern Mediterranean). Most typical values for the Curie discontinuity map for Israel are 42–46 km.

3   Tectono-Geophysical Examination

An integrated examination of geophysical data (GPS arrangement, geoid isolines, and oceanic block of the Earth's crust related to the Kiama epoch of inverse polarity), Mesozoic mantle rocks and minerals, and Cenozoic traps and orogenic volcanic complexes accompanied by regional tectonic setting are presented in Fig. 11. It should be noted that this map displays two geodynamic levels: (1) deep geodynamics associated with the core-lower mantle interaction (reflected in the geoid's data) and (2) comparatively subsurface geodynamics associated with the crust-upper mantle movements (reflected in the GPS data and crust-mantle magmatic
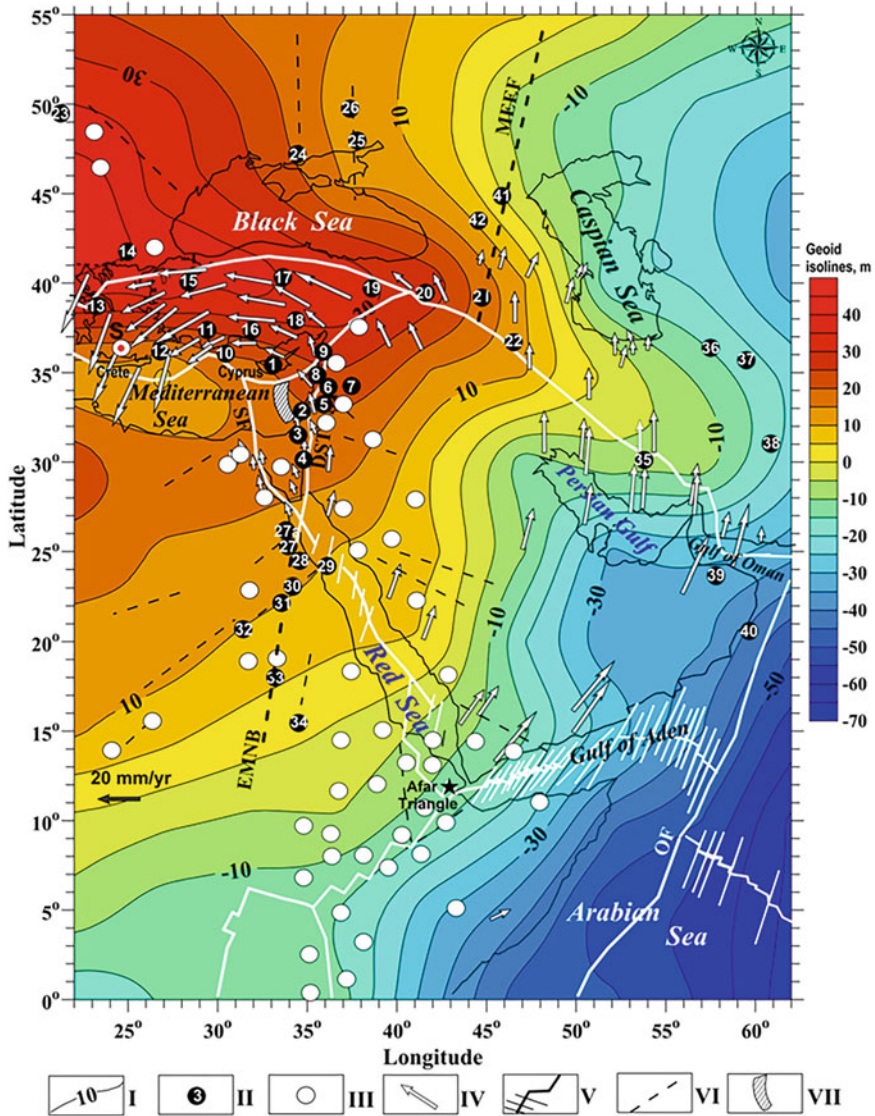
Fig. 11 Integrated geophysical-geological scheme of the region under study (after Eppelbaum and Katz 2017a, 2020, with modifications). (**I**) Generalized geoid's isolines (m) (constructed on the basis of the EMG2008 (Geoid isolines: https://earthobservatory.nasa.gov/Features/GRACE/page3. php)), (**II**) Outcrops of the Mesozoic mantle rocks and minerals: (1) Cyprus, (2) Mt. Carmel (N Israel), (3) Makhtesh Ramon (S Israel), (4) Timna (S Israel), (5) Jebel Sheqif (SW Syria), (6) Nabi-Matta (NW Syria), (7) Jebel Rmah (S Syria), (8) Baer-Bassit (NW Syria), (9) Kizildag (S Turkey), (10) Antalya, (SW Turkey), (11) Lycian (SW Turkey), (12) Karpathos-Rhodes (S Greece), (13) Locris-Beotia (Greece), (14) Krumovgrad (S Bulgaria), (15) Harmancik (NW Turkey), (16) Beysehir (S Turkey), (17) Ankara (Turkey), (18) Pozanti-Korsanti (S Turkey), (19) Tunceli (N Turkey), (20) Guleman (E Turkey), (21) Khoy-Maku (W Iran), (22) Kata-Rash (N Iraq), (23) Sedlica (E Slovakia), (24) Sivash (S Ukraine), (25) Priazov massif (S Ukraine), (26) Izium (E Ukraine), (27) Abukhruq (SE Egypt), (27a) Afia pipe, Wadi Zediun

events). Our computations (Fig. 4) indicate that the maximal entropy values derived from the satellite gravity field appear nearly the latitude of $35°$ to the North, i.e., nearly the critical parallel zone of the conjugate deformation of the Earth's ellipsoid (according to the Vèronnet theorem (Véronnet 1912)). The critical parameters of the $35°$ latitude were recently confirmed by Levin and Sasorova (2012) and Levin et al. (2013).

The western part of the region is distinguished from the eastern one by the variety of tectono-geodynamical indicators (GPS parameters (Fig. 11), Mesozoic terrane belt (see Fig. 3) anticlockwise movement), mineralogically (wide presence of diamonds (microdiamonds, moissanites, garnets, etc.)) (Greek Rhodope, Greece (Mposkos and Kostopoulos 2001); Tartous province, NW Syria (Mahfoud 2002); Makhtesh Ramon, S Israel (Eppelbaum et al. 2006); Wadi Zeidun, Central Eastern Desert (Egypt) (Barakat and Kandil 2019), Pozanti-Karsanti area, Turkey (Lian et al. 2017); Carmel, N Israel (Dobrzhinetskaya et al. 2018)), and petrologically (e.g., presence of rocks such as eclogites, dunites, peridotites, lherzolites, etc.) (Zabargad Is., Egypt (Bonatti et al. 1986); Baer-Bassit, NW Syria (Al-Riyami and Robertson 2002; Roure et al. 2012); Karpathos-Rhodes, S Greece (Dilek and Robinson 2003); Jebel Rmah, S Syria (Krasheninnikov et al. 2005); Kizildag, S Turkey (Okay et al. 2016)). Figure 11 also indicates division of the region into the western and eastern parts.

The latest combined geophysical-geological analysis (satellite-derived gravity data, gravity anomalies computation from the lower mantle, GPS pattern, paleomagnetic data, petrological-mineralogical examination, and tectono-structural reconstructions) allowed to recognize a giant quasi-ring lower-mantle structure within the area under study (Eppelbaum et al. 2020) (Fig. 12a). Figure 12b clearly indicates critical peculiarities of $35°$ latitude; these disturbances not only appear in the subsurface structure (tens of km) but also felt at the great depths (lower mantle).

Quantitative analysis of the residual gravity anomaly shown in Fig. 12a was carried out by the methods (improved characteristic point, tangent methods, and areal methods) specially developed for complex physical-geological conditions (Khesin et al. 1996; Eppelbaum and Khesin 2012): It was detected that the upper edge of this structure occurs at about 1700 km depth that corresponds to the lower mantle. GPS pattern and paleomagnetic and tectonic data clearly indicate

---

Fig. 11 (continued) (SE Egypt), (28) El Kahfa (SE Egypt), (29) Zabargad Is. (SE Egypt), (30) El Naga (SE Egypt), (31) Mansouri complex (SE Egypt), (32) Delgo (N Sudan), (33) Wadi Shaq Umm Bosh (E Sudan), (34) Mindara (E Sudan), (35) Neyriz (E Iran), (36) Sabzevar (NE Iran), (37) Torbat-e Heydarieh (E Iran), (38) Nehbandan (E Iran), (39) Semail (Oman), (40) Masirah (Oman), (41) Svetloyarskaya (SW Russia), (42) Kuban traps (N Caucasus, Russia), (**III**) Cenozoic traps and orogenic volcanic complexes, (**IV**) GPS velocity vectors (after Reilinger et al. 2006), (**V**) main interplate faults, (**VI**) main intraplate (predominantly radial) faults, (**VII**) Kiama paleomagnetic hyperzone of inverse polarity (Eppelbaum et al. 2014; Eppelbaum and Katz 2014, 2015b, c). Thin black lines show boundaries between the land and marine areas. *SF* Sinai Fault, *DST* Dead Sea Transform, *EMNB* Eastern Mediterranean Nubian Fault (Eppelbaum et al. 2018; Barakat and Kandil 2019), *MEEF* Main Eastern European Fault (Shatsky et al. 1956; Kopp 2004; Eppelbaum et al. 2018), *OF* Owen Fault
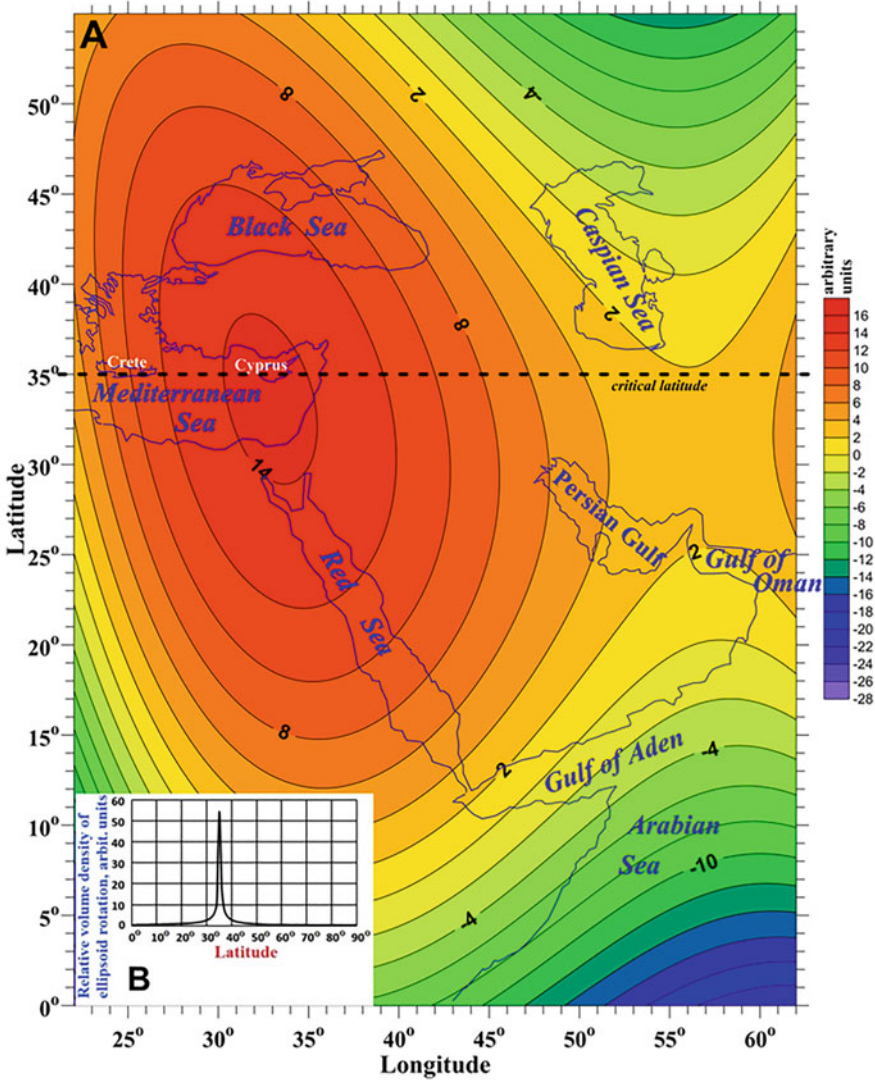
Fig. 12 (**a**) Cubic polynomial approximation of the satellite-derived gravity data (central part of the initial map is shown in Fig. 3) (after Eppelbaum et al. 2020, with modifications), (**b**) The dependence of the relative bulk density of the energy of rotation of the Earth's ellipsoid from latitude (after Levin et al. 2013)

counterclockwise rotation of this structure. Seismic tomography data confirm existence of velocity anomalies at this depth and above it (e.g., Wen and Helmberger 1998; Van der Meer et al. 2018). This anomaly sheds light on a number of phenomena including the Cyprus gravity anomaly, counterclockwise rotation of the Mesozoic terrane belt, and asymmetry of basins along the Dead Sea Transform

and Kiama tectonic unit movement lengthwise the regional transform faults (Eppelbaum et al. 2020).

The revealed deep quasi-ring structure is retracked in the topography field (see Fig. 2) and is reflected in many regional maps (for instance, in the basement depth map of the Arabian Plate (Konert et al. 2001)). Besides this, the Red Sea spreading coincides with long axis of the residual gravity anomaly (see Fig. 12a).

It is necessary to note that in the Cyprus Island (occurring in the geometrical center of the residual gravity anomaly (see Fig. 12a)), the high-amplitude (up to 200 mGal), but narrow gravity, Bouguer anomaly was registered (Gass 1968). Suetsugu et al. (2009) on the basis of seismic investigations in the South Pacific suggested a model of superplume from the lower mantle generating a series of small narrow plumes to relative subsurface. This model can relate to the considered case in the Eastern Mediterranean with the giant lower mantle structure and high-intensive, but comparatively narrow, Cyprus Bouguer gravity anomaly in its center (apparently produced by a small plume occurring at a relatively small depth below Cyprus).

Interestingly that a map of the satellite derived gravity coherence amplitude (see Fig. 6) shows clear quasi-circular anomaly just in the Cyprus area. It is necessary to note that the Crete Island geographic location also coincides with the critical 35° latitude (see Fig. 12a). Eppelbaum and Pilchin (2005) supposed that the catastrophic earthquake and tsunami accompanied by the Santorini volcano eruption in seventeenth century BC are the liable reasons of downfall of the Minoan Empire in the Crete Island. Some investigators consider that just the Minoan Empire was a legendary Atlantis.

The Easternmost Mediterranean (EMM) region (located in the NW part of the region) is characterized by several significant historical geological-geophysical events: (1) the Messinian crisis, (2) high seismicity, (3) active volcanism, (4) essential influence of sea level fluctuations and landscape changes to early hominid origin and evolution in Africa, and (5) uniqueness of the modern geological, geophysical, and climatic regional factors for creation of the greatest biospheric migrations from South to North and back (see Figs. 1 and 2).

According to modern geological-geophysical analyses, the EMM covers four geotectonic plates: the Nubian, Sinai, Arabian, and Aegean-Anatolian (Figs. 1 and 5). The Nubian and Sinai plates consist of heterogeneous blocks of oceanic and continental crust. Robertson et al. (1991) indicate that the oceanic crust of the EMM is a remnant of the Neotethys. The EMM is restricted from the east and west by two submeridional deep faults: the Dead Sea Transform (DST) and the Sinai Fault (SF) (Figs. 1 and 5). The DST formed the eastern part of the EMM. Along this transform, about 100 km of left-lateral strike-slip motion has developed (Garfunkel 1998). Between the continental and oceanic crust is situated the Syrian fold belt (Syrian arc) (e.g., Krasheninnikov et al. 2005). This belt is the eastern part of the larger Alpine-Mediterranean fold belt and basin system (Khain 2001). Analysis of subsurface Paleogene-Upper Cretaceous sediments indicates the structural inhomogeneity of the Syrian arc. However, the tectonic features of the deeper structural stages have been insufficiently studied. Ben-Avraham and Ginzburg (1990) have geophysically shown that the Syrian arc structure is composed of a thinned continental crust. Ben-Avraham et al. (2002, 2006) have tectonically found that this belt is

made up of a sequence of extensional independent crystal units. The aforementioned studies were accepted as a basis for further tectonic-geophysical integrated analysis. Map of gravity coherence amplitude (Fig. 6) that allows to delineate some tectono-structural units of the EMM is a component of such an analysis.

Precambrian, Paleozoic, Mesozoic, and Cenozoic associations form the geological section of the African and Arabian platforms within the EMM.

The Precambrian contains metamorphic and igneous rocks, and molasse was found in its upper part which passes to the Cambrian base. Cambrian rocks are widely found in Sinai but are not found in the borehole sections in the Negev desert. In the Negev, the Permian deposits overlie the Precambrian arkosic sandstone. No molasses were detected in the Heletz block, and the Permian deposits are in direct contact with the crystalline schist. More completely (comparing with Sinai), Lower Paleozoic sequences are present in the east of the EMM coast in Syria, Jordan, and Iran. Geophysical data examination testifies to the absence of Lower Paleozoic strata in Levant Basin and Pleshet terrane (Gardosh et al. 2010). Devonian and Carbon deposits have not been detected in the borehole sections of Israel. The Carbon and Permian continental associations were studied in Sinai (Hall et al. 2005). The deep boreholes drilled in the Negev, western Jordan, the coastal plain of Israel, and the Judean Mountains have revealed marine Permian deposits (Hall et al. 2005). Thus, the Precambrian and Paleozoic associations of the Arabian Plate and southern Sinai significantly differ from the folded zone of the Syrian arc.

The Mesozoic and Paleogene associations make up the carbonate platform of the EMM (including reefs and other organogenic constructions). These carbonate associations also include small terrigenous complexes and traps. The Mesozoic and Paleogene associations make up the carbonate platform of the EMM and sometimes contain reefs and other organogenic constructions. These carbonate associations also include small terrigenous complexes and traps. The Miocene and Quaternary associations are represented by terrigenous molasse with Early Messinian evaporates. These associations have developed mainly in the pull-apart basins within the DST and Levant Basin. In the EMM besides sedimentary deposits, Mesozoic and Late Cenozoic magmatic associations are widely developed (Garfunkel 1989; Segev 2009).

Robertson et al. (1991) proposed on the basis of examination of Mediterranean ophiolites of the Alpine belt that most ancient crust of the EMM corresponds to Late Triassic-Jurassic. The performed integrated geological-geophysical analysis (Eppelbaum et al. 2012, 2014; Eppelbaum and Katz 2011, 2012a, 2015b) and current research indicate that the southern side of the Neotethys Ocean, developed in the EMM, does not rather correspond to the known tectonic model of passive continental-ocean conjunction. Here are developed the Early Mesozoic terrane belt and remains of the oceanic crust (e.g., Triassic-Jurassic mélange) and accretionary prisms of the subducted Permian-Triassic oceanic crust. These data directly relate to the verification of location of the Kiama paleomagnetic hyperzone of inverse magnetization (Fig. 10) within the EMM. Basically, this is the first factual evidence of discovering ancient Late Paleozoic oceanic crust (260–280 Ma). We can also suggest that the Kiama hyperzone and the oceanic crust adjacent to it from the east may represent a part of "small oceanic basin." Ben-Avraham (1978) and

Ben-Avraham and Ginzburg (1990) noted that such tectonic structures exist in the EMM.

Jimenez-Munt et al. (2006) reconstructions demonstrate that within the EMM, the lithospheric thickness increases up to 125 km, while in the surrounding areas, this value is only about 100 km. This fact indicates the essential geodynamic activity during the Neotethys Ocean closing.

An uplift of continental crust blocks was situated to the west of the Neotethys in the modern EMM area (currently these blocks compose the Aegean-Anatolian belt (see Figs. 5 and 6) of the Neo-Tethyan collision zone). This uplift in the Jurassic triggered the biogeographical isolation of many assemblies of marine fauna of the Ethiopian province. The simultaneous extension of the Neotethys during the Jurassic and Paleotethys Ocean closing (e.g., Stampfli et al. 2013; Golonka and Ford 2000; Stampfli and Borel 2002) initiated an activation of block movements along a series of newly formed regional transform faults (Muttoni et al. 2003). A movement of composite elements of the terrane belt and partially conjugated blocks of Neotethys Ocean crust began along these transform faults in Late Jurassic-Early Cretaceous. At the same time, the geophysical data shown in the present chapter indicate that the western drift of the oceanic block of the southern side of Neotethys was accompanied by counterclockwise rotation of 90° that was discovered by the Kiama paleomagnetic hyperzone movement. This rotation was possibly strengthened at the final stages, while the Eratosthenes terrane was moved to the north. The discovery of the Kiama hyperzone (Eppelbaum et al. 2014) confirms the general conception of a remnant kind of the Earth's crust of the EMM which possibly represents at that time a "small ocean basin" (Ben-Avraham 1978; Robertson 1998). Presence of a submeridional-oriented thick lithosphere block (up to 125 km) in the EMM (Jimenez-Munt et al. 2006) roughly corresponds to the northern oceanic part of the Sinai Plate. This fact possibly reflects horizontal movement of deep crust-mantle blocks along a transition zone from the east to west during the time of the Neotethys Ocean development. The counterclockwise rotation of the discovered deep quasiring structure (see Figs. 11 and 12) confirms this proposition.

It is well-known that the age of oceanic crust is one of the most significant factors that determine its physical properties and many other geological-geophysical features (e.g., Khain 2001). The combined analysis of the geological-geophysical data in this region has been recognized as allochthonous in nature, both in the terrane belt and the oceanic crust zone of the EMM. The modern tectonic position of the terrane belt is associated with the Heletz Paleozoic structure (Weissbrod 2005). Our data indicate that up to Early Mesozoic, this terrane belt and the oceanic crust zone of the northern part of the Sinai Plate were formed to the east, approximately in the NW continuation of the Persian Gulf. The coastal line of the Ethiopian Sea of the Arabian foreland in Early Mesozoic approximately reached the modern western boundary of the Persian Gulf. Biogeographical data (presence of the Somalirhynchia-Septirhynchia fauna (Katz and Eppelbaum 1999) and structural-formational constructions (Eppelbaum and Katz 2015a, b) in general confirm this proposition.

Simple visual analysis indicates that most geodynamic activity in the region (Fig. 10) is confined to the greatest gradients of gravity field: the largest positive Bouguer gravity anomaly in the Cyprus and the highly negative Bouguer gravity
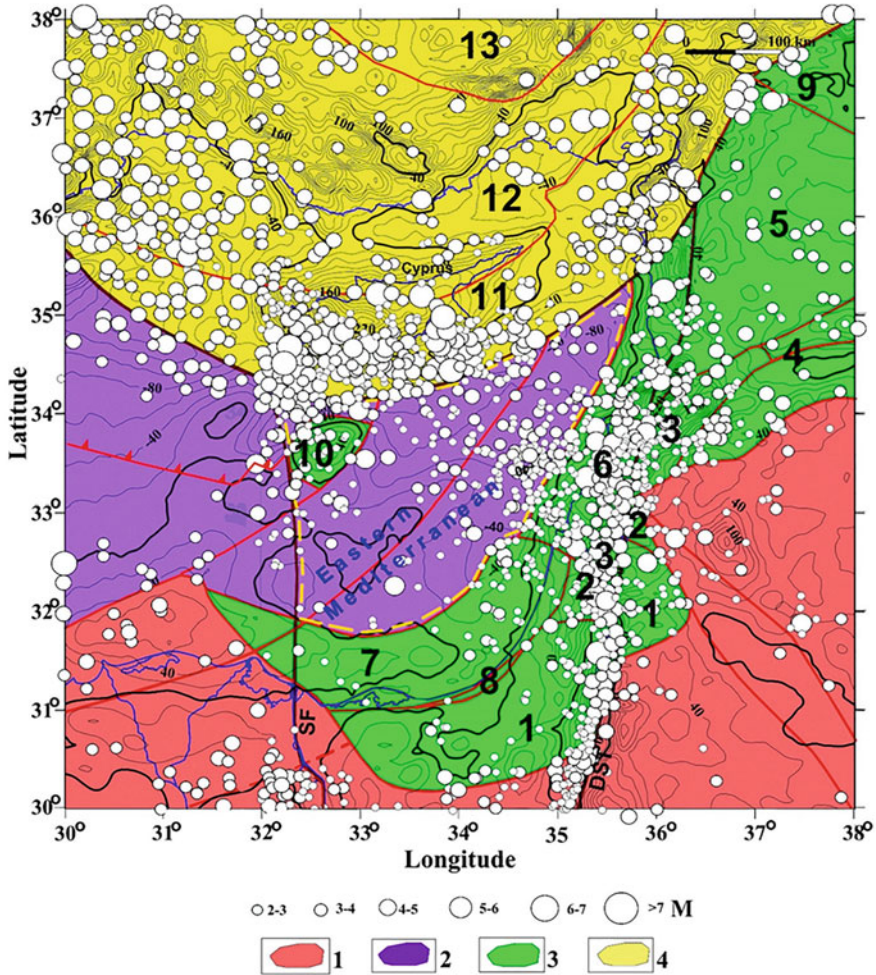
Fig. 13 Tectono-geodynamical map of the Easternmost Mediterranean with earthquake epicenters (for 1900–2012) (see magnitudes at the bottom of this figure) overlaid on the satellite-derived gravity map (isolines are given in mGals). Circles show the earthquake magnitudes by degree of increasing. (1) Precambrian crust, (2) Mesozoic oceanic crust, (3) Mesozoic terranes, (4) Alpine tectonic belt. Dotted yellow line displayed the position of the northern part of the Sinai Plate. Position of tectonic terranes (large black numbers): (1) Negev, (2) Judea-Samaria, (3) Anti-Lebanon, (4) Palmyride, (5) Aleppo, (6) Galilee-Lebanon, (7) Pleshet, (8) Heletz, (9) Abdelaziz, (10) Eratosthenes, (11) South Taurides, (12) Taurus, (13) Anatolides (after Eppelbaum and Katz (2015a), with modifications)

anomaly along the DST. Eppelbaum and Katz (2012b) have shown that gravity data retracked from the satellite observations can be employed for mapping the areas of dangerous geodynamic events. The boundaries of the African, Sinai, Arabian, and Aegean-Anatolian tectonic plates appear to be zones of higher activity. The Aegean-Anatolian Plate of the Alpine-Himalayan convergence zone is younger (Cenozoic) and characterized by more frequent and high-magnitude seismicity (Fig. 13). The

zones of the Mesozoic consolidation are seismically less active. However, the DST area, as was noted elsewhere (e.g., Arieh and Rabinowitz 1989; Ben-Avraham 1992), exhibits very active seismicity. The boundaries between the smaller tectonic-geophysical zones are identifiable but are less visible than the interplate boundaries. In particular, the boundaries of the Mesozoic terrane belt in contact with the continental crust of Gondwana and the thinned oceanic crust are fairly distinct, but not in all extensions. They developed mainly to the east and west of the DST.

4   Development of the Tectonic Map

The historical-planetological analysis indicates that the final phase of Paleozoic reflects the most extremal period of the Phanerozoic according to the degree of tectonothermal, paleomagnetic, hydrospheric, geodynamic, and climate-sedimentation activities (Lapkin and Katz 1990; Domeier et al. 2012). The stable tendency of geomagnetic regime to extensive direct-reverse polarity alteration was accompanied by essential thermal-geodynamic activity of lithosphere and upper mantle. This phenomenon reflects the convective geodynamics of plate tectonic relationships of Pangea and Panthalassa (e.g., Muttoni et al. 2009). According to the paleomagnetic reconstructions (Domeier et al. 2012; Muttoni et al. 2009), the geodynamic situation is considered within the models of the Late Permian Pangea A and Early Permian Pangea B. Figure 14 presents map of the Pangea B reconstruction (with the authors' additions).

This reconstruction unmistakably designates that the oceanic crust of Neotethys together with the framing terrane belts was situated to the east of the present area of the EMM. The main geodynamic feature of Pangea B is the triple plate junction, boundary of which corresponds to zones of spreading, subduction, and deep displacement (intra-Pangea dextral shear). Such displacements of blocks of continental and oceanic crust as well as blocks of mantle lithosphere at significant distances are known at different stages of the Neotethys Ocean evolution in the Late Mesozoic and Cenozoic (Stampfli et al. 2013; Jimenez-Munt et al. 2006; Burov 2011; Yamasaki and Stephenson 2011).

A generalized tectonic map of this region is of great necessity to solve different geological-geophysical, ecological, and other problems: tectono-geophysical mapping, development of 3D physical-geological models, searching different types of economic deposits, long-term seismological prognosis, solving some ecological and environmental problems, etc. Consequently, on the basis of comprehensive analysis of the following main publications, Glennie et al. (1990), Lenoir et al. (1994), Camelbeeck and Iranga (1996), Johnson (1998), Golonka and Ford (2000), Pollastro (2003), Alsharhan and Nairn (2004), Bosworth et al. (2005), Hall et al. (2005), Krasheninnikov et al. (2005), Reilinger et al. (2006), Al-Juboury and Al-Hadidy (2008), Bordenave (2008), Johnson and Kattan (2008), Johnson et al. (2008), Muttoni et al. (2009), Scotese (2009), Milesi et al. (2010), Stern and Johnson (2010), Verges et al. (2011), Eppelbaum and Katz (2012a, b), Moghadam et al.
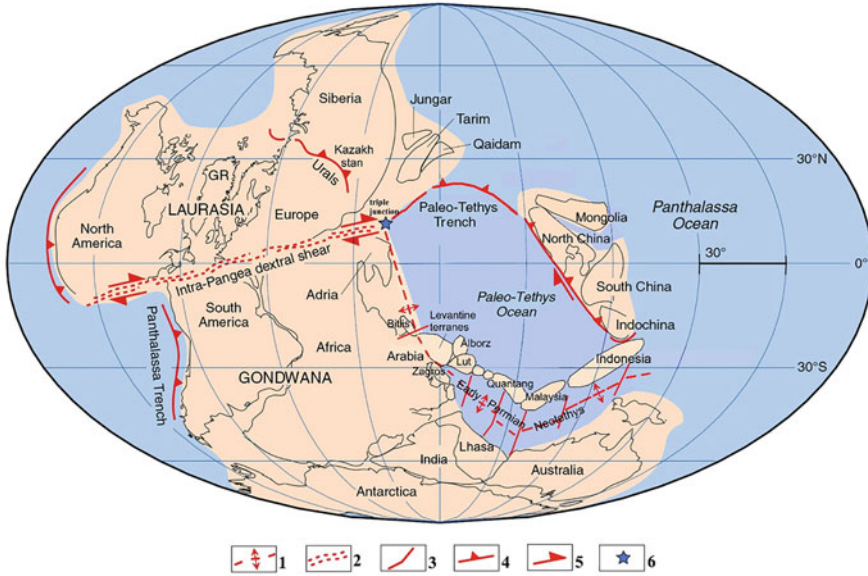
Fig. 14 Early Permian Neotethys position within the Pangea B-Panthalassa reconstruction (after Muttoni et al. 2009), with supplements from Stampfli et al. (2013), Golonka and Ford (2000), and some authors' supplements). (1) Neotethian ocean spreading center, (2) intra-Pangea dextral shear, (3) oceanic transform faults, (4) subduction zones, (5) direction of strike-slip motion, (6) triple junction (after Eppelbaum and Katz (2015a), with modifications)

(2013), Stampfli et al. (2013), Muluneh et al. (2014), Stamps et al. (2014), Eppelbaum and Katz (2015a), Tunini et al. (2015), Globig et al. (2016), Eppelbaum and Katz (2017a), Eppelbaum et al. (2018, 2020), and Van der Meer et al. (2018), and combined geophysical data examination, a new tectonic map of the Nubian-Arabian region has been developed (Fig. 15).

To develop the tectonic map, a classic method of such maps' construction—historical principle of structural evolution (e.g., Khain 2001)—was applied. For the first time, we show mosaics interaction of the tectonic units of three types: (1) active rift systems, (2) the basement structure of the African-Arabian platform, and (3) assembles of the northern boundary of this platform (including the firstly delineated Mesozoic-Cenozoic mobile belts). Some tectonic zonation results obtained for the oceanic crust (e.g., Bosworth et al. 2005; Eppelbaum and Katz 2015a, 2017a) are omitted due to the comparatively small scale of the compiled tectonic map (Fig. 15).

We must note that recently developed modern wavelet approaches for digital integration of different geophysical fields (Eppelbaum et al. 2011; Alperovich et al. 2013) will help, in the case of necessity, to create the joined 3D models of different blocks and regions.
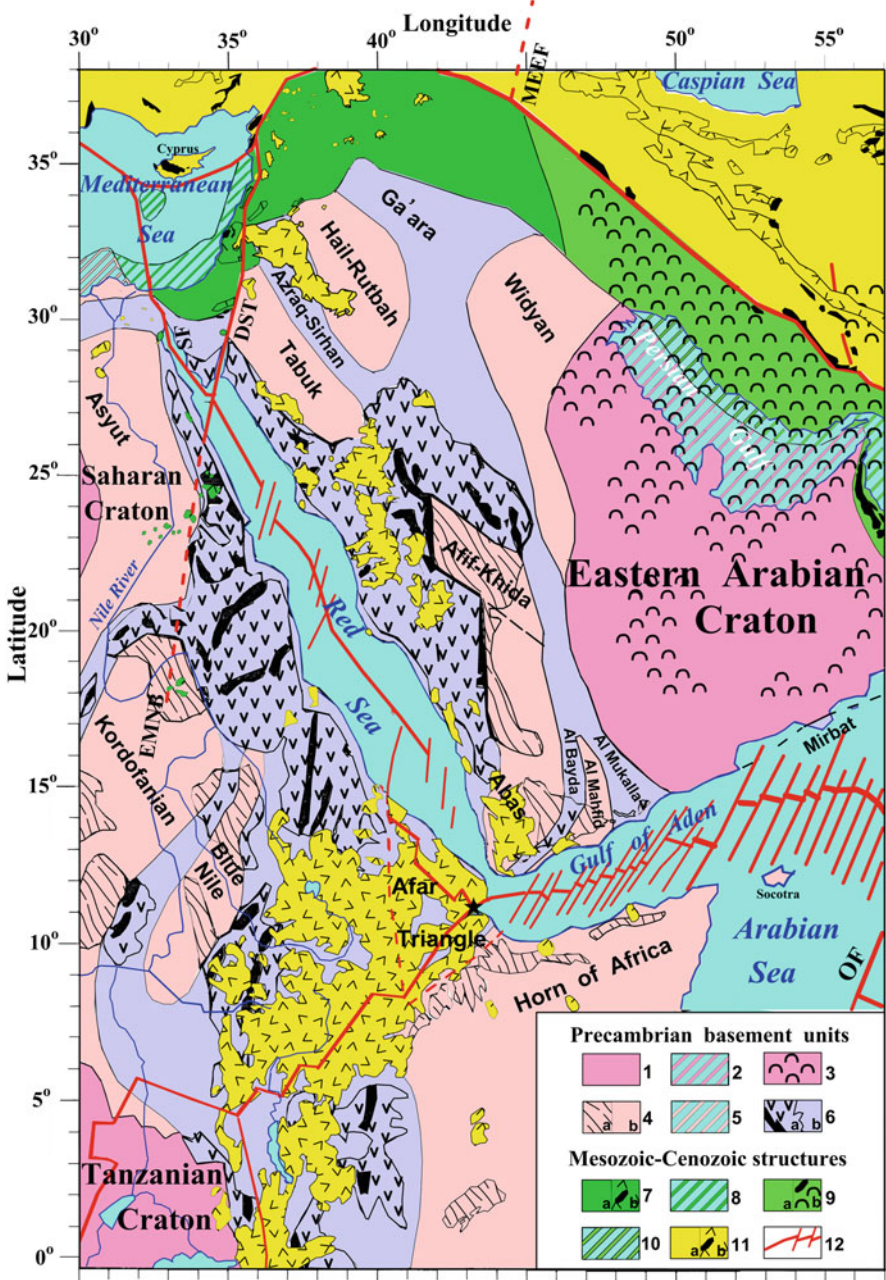
Fig. 15 A novel tectonic map of the region under study (after Eppelbaum and Katz 2017a, with modifications). (1) Archean cratons, (2) submarine continuation of Archean cratons, (3) Upper Precambrian salt basins, (4) Paleo-Mesoproterozoic basement: (a) exposed, (b) buried at the depth, (5) submarine continuation of Paleo-Mesoproterozoic basement, (6) Neoproterozoic belt: (a) exposed with ophiolites, (b) buried at the depth, (7) Early Cretaceous accretional complex:

5 Some Examples of Relationship Between Geophysical-Geodynamic Factors and Environments

The overwhelming impact of natural disasters to human health and the environment is self-evident. Climate significantly influences many of the Earth's physical and environmental characteristics, biological parameters, and social systems (e.g., Balling and Cerveny 1995; Cook et al. 1997; Huseynov and Guliyev 2004; Usoskin 2008; Reilly 2009; Scafetta 2010; Belleville et al. 2013; Higgins 2014; Wuebbles et al. 2014; Kohyama and Wallace 2016). Higgins (2014) notes that "The physical characteristics of the planet, the biological resources on which society depends, and our social systems have developed over a long time in response to climate conditions we're quickly leaving behind . . .".

Although the ratio of masses between the Sun and Moon consists of several orders of magnitude, the lunar contribution to the tidal variations is greater than the Sun, due to closer proximity of the Moon to the Earth (the Sun/Moon ratio of distances to the Earth is about 3.9×10^2) (Eppelbaum 2019). Many scientists have noted that the tidal variations and Wolf's number may trigger numerous significant environmental and geological processes on the Earth (e.g., Huseynov and Guliyev 2004; Neumeyer et al. 2006; Usoskin 2008; Alekseenko et al. 2009; Riguzzi et al. 2010; Levin and Sasorova 2012; Alizadeh et al. 2016). Some significant regional static gravity anomalies (their values range between several mGal and several hundreds of mGal) may also contribute to the dangerous climatic phenomena (Yaroshevich 2011; Ershova 2015).

Eppelbaum (2013) and Eppelbaum and Isakov (2015) have found a significant relationship between the cyclic Sun-Moon gravity-magnetic activity and number of tornadoes in Northern America. However, global warming and corresponding nonlinear weather changing interfere with this relationship.

Fig. 15 (continued) (a) traps and ophiolitic associations, (b) sedimentary rocks, (8) submarine continuation of the Early Cretaceous accretional complex, (9) Late Cretaceous accretional complex: (a) Neoproterozoic salts and Mesozoic ophiolites, (b) sedimentary deposits, (10) submarine continuation of Late Cretaceous accretional complex, (11) Cenozoic accretional and fault systems: (a) traps and ophiolites, (b) sedimentary rocks, (12) collisional and active rift systems. *EMNB* Eastern Mediterranean-Nubian Belt, *MEEF* Main Eastern European Fault, *SF* Sinai Fault, *DST* Dead Sea Transform, *OF* Owen Fault, *NWD* Northern Western Desert; symbol "filled star" designates triangle junction

5.1 Relationship Between the Geodynamics and Paleogeography

Geodynamic changes determined the development of biospheric transformations and the evolution of the Man. Among these fundamental events, four major occasions can be distinguished in the region under study (since Miocene).

1. The Messinian crisis (5.96 ± 0.02 million years ago) expressed in the strengthening of deep plate-tectonic processes that led to the closure of the Rifian Strait (Rifian corridor) (Chumakov 1967; de la Vara et al. 2016)—connecting the Mediterranean Sea with the Atlantic Ocean. It is interesting to note that firstly this phenomenon was discovered during the construction of the Aswan hydroelectric station in Egypt (Chumakov 1967). We can suggest the giant deep quasiring counterclockwise rotating structure centered below the Cyprus Island (see Fig. 12a) (Eppelbaum et al. 2020) had a certain impact to this process. The Messinian crisis led to the drainage of the Mediterranean Sea, dramatic climatic and biospheric transformations, and the beginning of the evolution of hominids that changed their habitat. The consequence of this was a change in hominid lifestyle and a radical change in physiology, morphology, and a boom in cephalization and brain evolution.

2. The Middle Akchagyl Sea Transgression (up to +200 m) (e.g., Alizadeh et al. 2016) has flooded the protoareals of *Homo erectus* in the Eastern Africa 2 million years ago. Just for this flat area (see Fig. 2), such extensive flooding could be a very significant factor in the need for migration of *Homo erectus* and many representatives of the fauna. Apparently, it was the main reason of the expansion of the *Homo erectus* habitat migration through geomorphologically elevated sections of the Mesozoic terrane belt (see Figs. 2, 3, and 4) to the zones of optimal landscapes in the Transcaucasus and Central Asia. Uplifted position of the Mesozoic terrane belt in Neogene follows from paleogeographical map presented in Eppelbaum and Katz (2015b) (Fig. 12 in the mentioned article: Map of the Neogene-Quaternary structural stage of the Eastern Mediterranean).

3. The Late Pleistocene (60–10 thousand years ago) era of the formation of the modern type of climatic zonality and biosphere landscapes in the conditions of glacial drainage of the shelf zones. At the same time, two large civilizational development centers of *Homo sapiens* arose in our region—on the shelf of the Mediterranean Sea and the Arabian-Indian Ocean shelf. The probable development of a sufficiently powerful technocratic civilization that possessed the technical capabilities for the marine navigation and transfer to many thousands of kilometers—to the zones of Australia, New Zealand, and the Pacific Islands—dates to this period.

4. The Holocene interglacial flooding of the shelf (about 10,000 years ago), which led to the colonization of the surrounding shelf of high plateaus, river valleys, and mountain ranges. Here new civilization centers developed on the basis of the merger of shelf technocratic and autochthonous indigenous cultures. Ultimately,

this led to the expansion of the oecumene and the merger of its Arabian-Mediterranean area with the East Asian and further to the migration of the Man into the New World, where elements as Paleo-Asian (Mongoloid) and Arabian-Indo-Oceanic (Vedoid) penetrated.

5.2 Relationship Between the Solar Activity and Mud Volcanism

Irregular degassing of the Earth is a fundamental feature of its evolution reflecting in tectonic and sedimentation cycles, sea level fluctuations, accumulation of mineral resources, and other phenomena. This peculiarity of global-scale Earth degassing is related to cosmic and endogenic rhythms or cycles, such as the short periodicity of rhythmic hydrocarbon gassing (Guliyev 2005). The rhythms of hydrocarbon degassing are most obviously manifested in the periodicity of eruptions and activity of mud volcanoes which are accompanied by the release of hundreds of millions of cubic meters of methane, oil, and groundwater. The periodicity in eruptions established for a sufficiently long time interval indicates a stable correlation between the solar activity and mud volcanism from one side, Caspian Sea level fluctuations, and seismicity from the second side (Guliyev 2005) (Fig. 16).

5.3 Relationship Between the Geological Epochs, Hydrospheric Disturbances and Paleomagnetic Reversals

The conventional geological cycles in the Earth may consist of several and tens of thousands to millions of years (cyclicity of tectonic and endogenic processes is analyzed in detail in Aleinikov et al. (2001)). Figure 17 shows an intricate relationship between the geological epochs, sinking ocean level, and paleomagnetic reversals (cycles).

Here are the most important geological periods associated with the development of the humankind.

M: The Messinian crisis (regression between 5.7–5.4 million years ago) dramatically affected the development of the basins, climate and ecosystems of the African-Arabian region. The phenomenon of hominization, the development of bipedal locomotion and the first producing anthropic societies are the essential properties of this stage.

A: The Akchagyl flooding of the ecosystems of the habitat of *Homo habilis* and *H*. erectus (about 2 million years ago) led to the first transcontinental migration of hominids.

P: A sharp Pleistocene drop in sea level (0.844 million years ago) against the background of equatorial regression and the development of continental glaciations
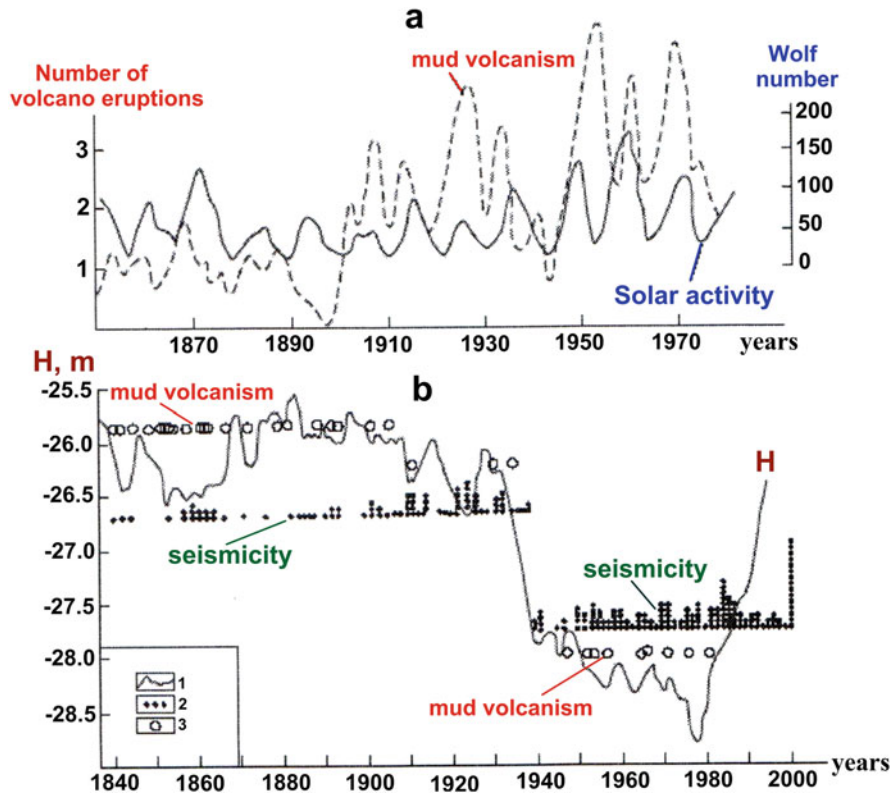
Fig. 16 Relationships between the mud volcanism and some periodical natural processes in the South Caspian Basin (after Guliyev (2005), with modifications). (**a**) comparison of solar activity (Wolf number) and mud volcanism, (**b**) comparison of mud volcanism with the Caspian Sea level fluctuations and seismicity. (1) Caspian Sea level fluctuations, H (in **b**), (2) seismicity, (3) mud volcanism (in **a** and **b**)

led to the beginning of sapientization of hominids and their influence on the surrounding ecosystems of the biosphere.

H: Noospherization of *Homo sapiens* began from the end of the Pleistocene (about 60,000 years ago)—the beginning of the Holocene (about 10,000 years ago) and was marked by the development of polis-technocratic civilizations and the development of navigation. At this time has been formed an ethnosphere which by the beginning of the Holocene covered all continents and islands of the oceanic space.
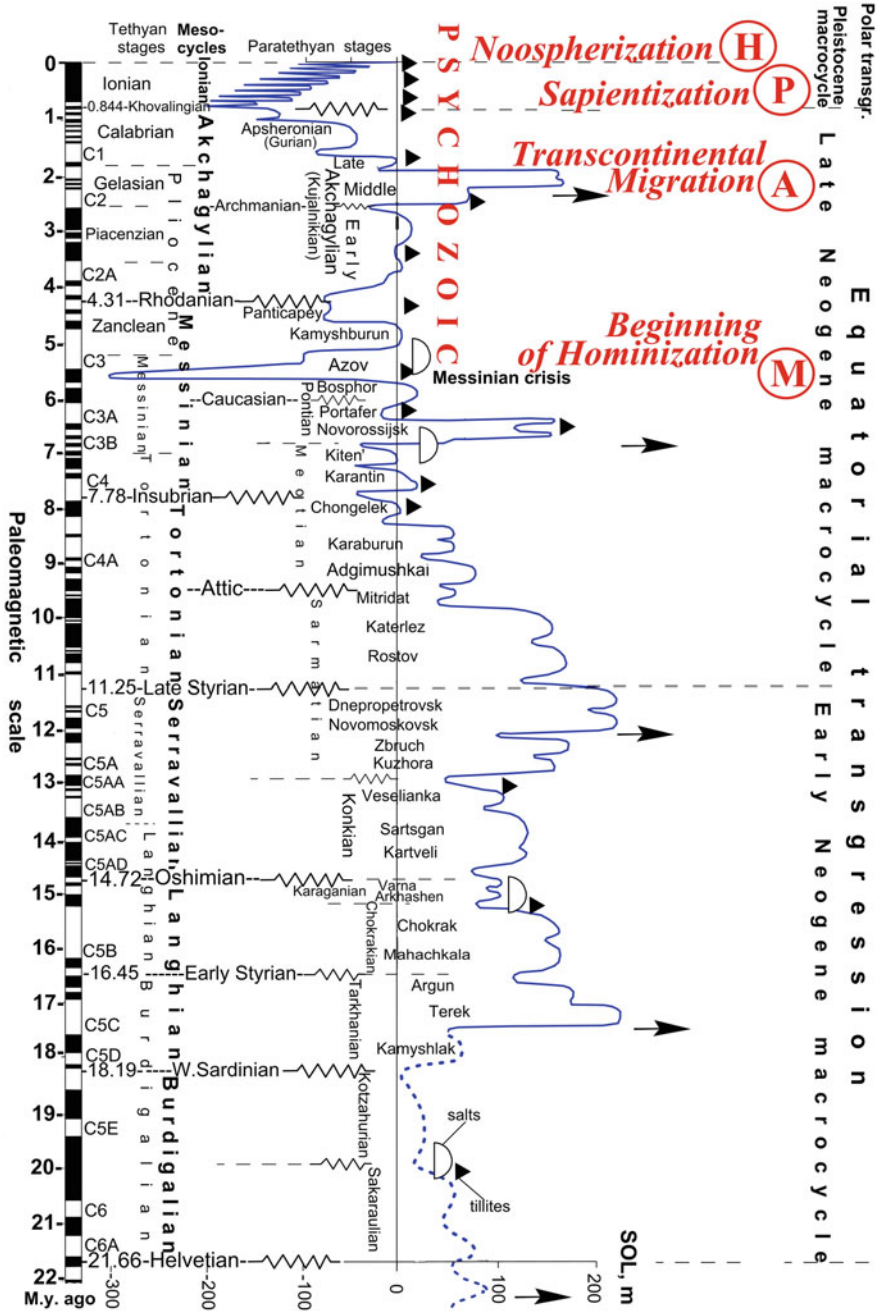
Fig. 17 Relationship between geological epochs, sinking ocean level, and paleomagnetic reversals during Neogene (from Y.I. Katz' unpublished book "A Cyclic System of Geological Time Scale", with modifications). SOL, standard ocean level, H, Holocene, P, Pleistocene, A, Akchagylian, M, Messinian

6 Conclusions

Without hesitation, deep structure elements influence all near-surface and surface processes, including natural, economical, and historical factors. However, their impact often is masked by many accompanying factors. The performed analysis shows intricate pattern of geological-geophysical data reflecting very multifarious deep structure of the entirely Nubian-Arabian region and its western-northern part—Easternmost Mediterranean. Here were considered mainly three potential geophysical fields (gravity, magnetic, and thermal), map of paleomagnetic reconstructions, and seismology map (the last two maps for the Easternmost Mediterranean region) as well as field of terrain relief. Relationship of the fields with geodynamic and tectonic factors, between themselves, and with the environments are very complex. The performed geophysical data interpretation enables to select various sectors of the region characterized by the different properties, but their influence to the natural, biological, historical, and climatic factors has a pronounced multiparameter character and is a subject of further comprehensive combined investigations.

References

Aleinikov AL, Belikov VT, Eppelbaum LV (2001) Some physical foundations of geodynamics (in Russian, contents and summary in English). Kedem Printing-House, Tel Aviv

Alekseenko VV, Gavrilyuk YM, Gromushkin DM, Dzhappuev DD, Kudzhaev AU, Kuzminov VV, Mikhailova OI, Stenkin YV, Stepanov VI (2009) Correlation of variations in the thermal neutron flux from the Earth's crust with the Moon's phases and with seismic activity. Izv Phys Solid Earth 45(8):709–718

Alizadeh AA, Guliyev IS, Kadirov FA, Eppelbaum LV (2016) Geosciences of Azerbaijan, vols I & II. Springer, Heidelberg

Al-Juboury A, Al-Hadidy A (2008) Facies and depositional environments of the Devonian-carboniferous succession of Iraq. Geol J 43:383–396

Alperovich L, Eppelbaum L, Zheludev V, Dumoulin J, Soldovieri F, Proto M, Bavusi M, Loperte A (2013) A new combined wavelet methodology applied to GPR and ERT data in the Montagnole experiment (French Alps). J Geophy Eng 10(2):025017, 1–17

Al-Riyami K, Robertson A (2002) Mesozoic sedimentary and magmatic evolution of the Arabian continental margin, Northern Syria: evidence from the Baer–Bassit Mélange. Geol Mag 139:395–420

Alsharhan AS, Nairn AEM (2004) Sedimentary basins and petroleum geology of the Middle East. Elsevier, Amsterdam

Andersen OB, Knudsen P, Berry PAM (2009) The DNSC-08GRA global marine gravity field from double retracked satellite altimetry. J Geodesy 84(3):191–199

Arieh E, Rabinowitz N (1989) Probabilistic assessment of earthquake hazard in Israel. Tectonophysics 167:223–233

Artemieva IM (2006) Global 1° x 1° thermal model TC1 for the continental lithosphere: implications for lithosphere secular evolution. Tectonophysics 416:245–277

Artemieva I, Thybo H, Kaban MK (2006) Deep Europe today: geophysical synthesis of the upper mantle structure and lithospheric processes over 3.5 Ga. In: Gee D, Stephenson R (eds) Special volume: European lithosphere dynamics. Geol Soc Lond 32:11–41

Balling RC, Cerveny RS (1995) Influence of Lunar phase on daily global temperatures. Science 267 (5203):1481–1483

Barakat AA, Kandil SMR (2019) Diamond in the newly discovered kimberlite and related rocks, Central Eastern Desert, Egypt. In: Proceedings of the XXXVI international conference of "Magmatism of the Earth and related strategic metal deposits", St Petersburg University, Russia, 23–26 May 2019, pp 36–42

Bastow ID, Keir D, Daly E (2011) The Ethiopia Afar Geoscientific Experiment (EAGLE): probing the transition from continental rifting to incipient seafloor spreading. In: Beccaluva L, Bianchini G, Wilson M (eds) Volcanism and evolution of the African Lithosphere. The Geological Society of America, Special paper 478, pp 51–76

Belleville G, Foldes-Busque G, Dixon M, Marquis-Pelletier É, Barbeau S, Poitras J, Chauny J-M, Diodati JG, Fleet R, Marchand A (2013) Impact of seasonal and lunar cycles on psychological symptoms in the ED: an empirical investigation of widely spread beliefs. Gen Hosp Psychiatry 35:192–194

Ben-Avraham Z (1978) The structure and tectonic setting of the Levan continental margin, Eastern Mediterranean. Tectonophysics 46:313–331

Ben-Avraham Z (1992) Development of asymmetric basins along continental transform faults. Tectonophysics 215:209–220

Ben-Avraham Z, Ginzburg A (1990) Displaced terranes and crustal evolution of the Levant and the Eastern Mediterranean. Tectonics 9:613–622

Ben-Avraham Z, Ginzburg A, Makris J, Eppelbaum L (2002) Crustal structure of the Levant basin, Eastern Mediterranean. Tectonophysics 346:23–43

Ben-Avraham Z, Schattner U, Lazar M, Hall JK, Ben-Gai Y, Neev D, Reshef M (2006) Segmentation of the Levant continental margin, Eastern Mediterranean. Tectonics 25(TC5002):1–17

Blaser N, Guskov SI, Entin VA, Wolfer DP, Kanevskyi VA, Lipp H-P (2014) Gravity anomalies without geomagnetic disturbances interfere with pigeon homing—a GPS tracking study. J Exp Biol 217:4057–4067

Bonatti E, Ottonello G, Hamlyn PR (1986) Peridotites from the Island of Zabargad (St. John), Red Sea: petrology and geochemistry. J Geophys Res 91(B1):599–631

Bordenave ML (2008) The origin of the Permo-Triassic gas accumulations in the Iranian Zagros foldbelt and contiguous offshore areas: a review of the Paleozoic petroleum system. J Pet Geol 31(1):3–42

Bosworth W, Huchon P, McClay K (2005) The Red Sea and Gulf of Aden Basins. J Afr Earth Sci 43:334–378

Braitenberg C, Ebbing J (2009) New insights into the basement structure of the West Siberian Basin from forward and inverse modeling of GRACE satellite gravity data. J Geophys Res 114 (B06402):1–15

Braun J (2010) The many surface expressions of mantle dynamics. Nat Geosci 3:825–833

Burov EB (2011) Rheology and strength of the lithosphere. Mar Pet Geol 28:1402–1433

Camelbeeck T, Iranga MD (1996) Deep crustal earthquakes and active faults along the Rukwa trough, Eastern Africa. Geophys J Int 124:612–630

Cermak V (1993) Lithospheric thermal regimes in Europe. Phys Earth Planet Inter 79:179–193

Cermak V, Rybach L (eds) (1991) Terrestrial heat flow and lithosphere structure. Springer, Berlin

Chumakov IS (1967) Pliocene and Pleistocene deposits of the Nile Valley in Nubia and Upper Egypt. Trans Geol Inst Sov Acad Sci 170:1–113

Cloetingh S, Willet SD (2013) Linking deep Earth and surface processes. Eos 94(5):53–54

Cook ER, Meko DM, Stockton CW (1997) A new assessment of possible solar and lunar forcing of bidecadal drought rhythm in the Western United States. J Clim 10:1343–1356

Davis PM, Slack PD (2002) The uppermost mantle beneath the Kenya dome and relation to melting, rifting and uplift in East Africa. Geophys Res Lett 29(7):1117, 1–4

de la Vara A, van Baak CCC, Marzochii A, Grothe A, Meijer PT (2016) Quantitative analysis of Paratethys Sea level change during the Messinian Salinity Crisis. Mar Geol 379:39–51

Dilek Y, Robinson RT (eds) (2003) Ophiolites in Earth history. The Geological Society of America, London, p 218. Special Publication

Dobrzhinetskaya L, Mukhin P, Wang Q, Wirth R, Zhao W, Eppelbaum L, Sokhonchuk T, Green H (2018) Moissanite (SiC) with metal-silicide and silicon inclusions from tuff of Israel: search for a primary source. Lithos 310–311:355–368

Domeier M, Van der Voo R, Torsvik T (2012) Paleomagnetism and Pangea: the road to reconciliation. Tectonophysics 514-517:14–43

Eckstein Y (1978) Review of heat flow data from the Eastern Mediterranean region. Pure Appl Geophys 117:150–159

Elgabry MN, Panza GF, Badawy AA, Ibrahim MK (2013) Imaging a relic of complex tectonics: the lithosphere-asthenosphere structure in the Eastern Mediterranean. Terra Nova 25:102–109

Eppelbaum LV (2013) Non-stochastic long-term prediction model for US tornado level. Nat Hazards 69(30):2269–2278

Eppelbaum LV (2015) Comparison of 3D integrated geophysical modeling in the south Caucasian and Eastern Mediterranean segments of the Alpine-Himalayan tectonic belt. Izv Acad Sci Azerb Rep Ser Earth Sci 3:25–45

Eppelbaum LV (2017a) Satellite gravimetry ('big data'): a powerful tool for regional tectonic examination and reconstructions. In: Veress B, Szigethy J (eds) Horizons in Earth science research, vol 17. Nova Science, New York, pp 54–86

Eppelbaum LV (2017b) From micro- to satellite gravity: understanding the Earth. Am J Geogr Res Rev 1(3):1–34

Eppelbaum LV (2019) Geophysical potential fields: geological and environmental applications. Elsevier, Amsterdam

Eppelbaum L, Isakov A (2015) Implementation of the geo-correlation methodology for predictability of catastrophic weather events: long-term US tornado season and short-term hurricanes. Environ Earth Sci 74:3371–3383

Eppelbaum LV, Kardashov VR (2001) Analysis of strongly nonlinear processes in geophysics. In Moresi L, Müller D (eds) In: Proceedings of the chapman conference on exploration geodynamics, Dunsborough, pp 43–44

Eppelbaum L, Katz Y (2011) Tectonic-geophysical mapping of Israel and Eastern Mediterranean: implication for hydrocarbon prospecting. Positioning 2(1):36–54. https://doi.org/10.4236/pos.2011.21004

Eppelbaum LV, Katz YI (2012a) Mineral deposits in Israel: a contemporary view. In Ya'ari A, Zahavi ED (eds) Israel: social, economic and political developments. Nova Science Publishers, New York, pp 1–41

Eppelbaum LV, Katz YI (2012b) Key features of seismo-neotectonic pattern of the Eastern Mediterranean. Izv Acad Sci Azerb Rep Ser Earth Sci 3:29–40

Eppelbaum LV, Katz YI (2014) First paleomagnetic map of the Easternmost Mediterranean derived from combined geophysical-geological analysis. Transactions of the 10th EUG Meeting, Geophysical Research Abstracts, vol 16, EGU2014-2424, Vienna, pp 1–5

Eppelbaum LV, Katz YI (2015a) Newly developed paleomagnetic map of the Easternmost Mediterranean unmasks geodynamic history of this region. Central Eur J Geosci (Open Geosci) 7 (1):95–117

Eppelbaum LV, Katz YI (2015b) Eastern Mediterranean: combined geological-geophysical zonation and paleogeodynamics of the Mesozoic and Cenozoic structural-sedimentation stages. Mar Pet Geol 65:198–216

Eppelbaum LV, Katz YI (2015c) Paleomagnetic mapping in various areas of the Easternmost Mediterranean based on an integrated geological-geophysical analysis. In: Eppelbaum L (ed) New developments in Paleomagnetism research. Earth Sciences in the 21st century. Nova Science Publisher, New York, pp 15–52

Eppelbaum LV, Katz YI (2017a) A new regard on the tectonic map of the Arabian-African region inferred from the satellite gravity analysis. Acta Geophys 65:607–626

Eppelbaum LV, Katz YI (2017b) Advanced Paleomagnetic mapping unmasks tectonic pattern of the Easternmost Mediterranean. Transactions of the AAPG European regional conference of

"Hydrocarbons in the Mediterranean: revisiting mature plays and understanding new and emerging ideas". Larnaca, Cyprus

Eppelbaum LV, Katz YI (2017c) Some tectono-geodynamical features of the Eurasian-African region. Transactions of the Vth international conference of "Geology and hydrocarbon potential of the Balkan-Black Sea region". Varna, Bulgaria, pp 13–20

Eppelbaum L, Katz Y (2020) Significant tectono-geophysical features of the African-Arabian tectonic region: an overview. Geotectonics (Springer) 54(2):266–283

Eppelbaum LV, Khesin BE (2012) Geophysical studies in the Caucasus. Springer, Heidelberg

Eppelbaum LV, Pilchin AN (2005) A quick subsidence of a crustal block in SW Aegean Sea as a possible cause of the end of ancient civilization in 17th century BC. Transactions of the international conference of "Atlantis hypothesis: searching for a lost land", Milos Island

Eppelbaum LV, Pilchin AN (2006) Methodology of Moho discontinuity map development for regions with low thermal characteristics: an example from Israel. Earth Planet Sci Lett 243 (3–4):536–551

Eppelbaum LV, Vaksman VL, Kouznetsov SV, Sazonova LM, Smirnov SA, Surkov AV, Bezlepkin B, Katz Y, Korotaeva NN, Belovitskaya G (2006) Discovering of microdiamonds and minerals-satellites in Canyon Makhtesh Ramon (Negev desert, Israel). Dokl Earth Sci 407 (2):202–204

Eppelbaum LV, Alperovich L, Zheludev V, Pechersky A (2011) Application of informational and wavelet approaches for integrated processing of geophysical data in complex environments. In: Proceedings of the 2011 SAGEEP Conference, Charleston, South Carolina, vol 24, pp 24–60

Eppelbaum LV, Katz YI, Ben-Avraham Z (2012) Israel—petroleum geology and prospective provinces. AAPG Eur Newslett 4:4–9

Eppelbaum LV, Nikolaev AV, Katz YI (2014) Space location of the Kiama paleomagnetic hyperzone of inverse polarity in the crust of the Eastern Mediterranean. Dokl Earth Sci 457 (6):710–714

Eppelbaum L, Katz Y, Klokochnik J, Kosteletsky J, Zheludev V, Ben-Avraham Z (2018) Tectonic insights into the Arabian-African region inferred from a comprehensive examination of satellite gravity big data. Glob Planet Chang 171:65–87

Eppelbaum LV, Katz Y, Ben-Avraham Z (2019) New data of the geodynamic evolution of the Eastern Mediterranean. AAPG conference of "Exploration and development of siliciclastic and carbonate reservoirs in the Eastern Mediterranean". Tel Aviv

Eppelbaum LV, Ben-Avraham Z, Katz Y, Cloetingh S, Kaban M (2020) Combined multifactor evidence of a Giant lower-mantle ring structure below the Eastern Mediterranean. Positioning 11:11–32

Erickson AJ, Simmons G, Ryan WBF (1977) Review of heat flow data from the Mediterranean and Aegean Seas. In: Biju-Duval B, Montadert L (eds) International Symposium on the structural history of the Mediterranean Basins, 25th Geological Congress, Technip, Splite, pp 263–280

Ershova TB (2015) Space inhomogeneity of the thunderstorm activity and Earth's gravity field anomalies. Bull Tomsk State Ped Univ 11(164):169–173. (in Russian)

Förster HJ, Förster A, Oberhansli R, Stromeyer D (2010) Lithospheric composition and thermal structure of the Arabian Shield in Jordan. Tectonophysics 481(104):29–37

Gaina C, Torsvik TH, van Hinsbergen DJJ, Medvedev S, Werner SC, Labails C (2013) The African plate: a history of oceanic crust accretion and subduction since the Jurassic. Tectonophysics 604:4–25

Gardosh MA, Garfunkel Z, Druckman Y, Buchbinder B (2010) Tethyan rifting in the Levant region and its role in early Mesozoic crustal evolution. Geolog Soc Lond 341:9–36

Garfunkel Z (1989) Tectonic setting of Phanerozoic magmatism in Israel. Isr J Earth Sci 38 (2–4):51–74

Garfunkel Z (1998) Constrains on the origin and history of the Eastern Mediterranean basin. Tectonophysics 298(1–3):5–35

Gass IG (1968) Is the Troodos Massif of Cyprus a fragment of Mesozoic ocean floor? Nature 220:39–42

Geoid Isolines. https://earthobservatory.nasa.gov/Features/GRACE/page3.php. Last visited on 14 Apr 2020

Glennie KW, Clarke MWH, Boeuf MGA, Pilaar WFH, Reinhardt BM (1990) Inter-relationship of Makran-Oman Mountains belts of convergence. In: Robertson AHF, Searle MP, Ries AC (eds) The geology and tectonics of the Oman region, vol 49. Geological Society, London, Special Publications, pp 773–786

Globig J, Fernandez M, Torne M, Verges J, Robert A, Facenna C (2016) New insights into the crust and lithospheric mantle structure of Africa from elevation, geoid, and thermal analysis. J Geophys Res Solid Earth 121:1–36. https://doi.org/10.1002/2016JB012972

Golonka J, Ford D (2000) Pangean (late carboniferous—middle Jurassic) paleoenvironment and lithofacies. Palaeogeogr Paleoclimatol Paleoecol 161:1–34

Gould JL (2017) Animal navigation: a novel map strategy. Curr Biol 27:R833–R852

Guliyev IS (2005) Mud volcanism in Azerbaijan. In: Ismailzadeh AT (ed) Recent geodynamics, georisk and sustainable development in the Black Sea to Caspian Sea Region. In: Proceedings of the International Workshop, AIP Conference Proceeding, vol 825, Baku, pp 11–18

Hall JK, Krasheninnikov VA, Hirsch F, Benjamini C, Flexer A (eds) (2005) Geological framework of the Levant, vol 2. The Levantine Basin and Israel, Jerusalem

Hansen SE, Rodgers AJ, Schwartz SY, Al-Amri AMS (2007) Imaging ruptured lithosphere beneath the Red Sea and Arabian Peninsula. Earth Planet Sci Lett 259:256–265

Hershkovitz I, Weber GI, Quam R et al (2018) The earliest modern humans outside Africa. Science 359:456–459

Higgins P (2014) How to deal with climate change. Phys Today 67(10):32–37

Huseynov DA, Guliyev IS (2004) Mud volcanic natural phenomena in the South Caspian Basin: geology, fluid dynamics and environmental impact. Environ Geol 46:1012–1023

Jimenez-Munt I, Sabadini R, Gardi A (2006) Active deformation in the Mediterranean from Gibraltar to Anatolia inferred from numerical modeling and geodetic and seismological data. J Geophys Res 108(B1):1–24

Johnson PR (1998) Tectonic map of Saudi Arabia and adjacent areas. Deputy Ministry for Mineral Resources, USGS -TR-98-3, Saudi Arabia

Johnson PR, Kattan FH (2008) Lithostratigraphic revision in the Arabian shield: the impacts of geochronology and tectonic analysis. Arab J Sci Eng 33(1):3–16

Johnson PR, Kattan FH, Al-Saleh AM (2008) Neoproterozoic ophiolites in the Arabian shield: field relations and structure, chapter 4. In: Kusky TM (ed) Precambrian ophiolites and related rocks, developments in precambrian geology, vol 13, pp 129–162

Katz YI, Eppelbaum LV (1999) Levantine phase of tectonic-thermal activity in the Eastern Mediterranean. Trans Ann Meet Geol Soc Am. Sect: Planet Geol 31:7, A119

Khain VE (2001) Tectonics of continents and oceans. Scientific World, Moscow. (in Russian)

Khalilov E (2011) Natural hazards and global problems of the modern civilization. Geocataclysm, Moscow. (in Russian)

Khesin BE, Alexeyev VV, Eppelbaum LV (1996) Interpretation of geophysical fields in complicated environments. Modern approaches in geophysics. Kluwer Academic, Boston

Klokočník J, Kostelecký J, Eppelbaum L, Bezděk A (2014) Gravity disturbances, the Marussi tensor, invariants and other functions of the geopotential represented by EGM 2008. J Earth Sci Res 2(3):88–101

Kohyama T, Wallace JM (2016) Rainfall variations induced by the lunar gravitational atmospheric tide and their implications for the relationship between tropical rainfall and humidity. Geophys Res Lett 43:918–923

Konert G, Afifi AM, Al-Harjri SA, Droste HJ (2001) Paleozoic stratigraphic and hydrocarbon habitat of the Arabian Plate. GeoArabia 6:407–442

Kopp ML (2004) Mobilistic theory of platforms of South-Eastern Europe. Nauka, Moscow. (in Russian)

Korostelev F, Basuyau C, Leroy S, Tiberi C, Ahmed A, Stuart GW, Keir D, Rolandone F, Al Ganad F, Khanbari K, Boschi L (2014) Crustal and upper mantle structure beneath South-Western margin of the Arabian Peninsula from teleseismic tomography. Geochem Geophys Geosyst 15:2850–2864

Krasheninnikov VA, Hall JK, Hirsch F, Benjamini H, Flexer A (eds) (2005) Geological framework of the Levant, vol 1. Cyprus and Syria, Jerusalem

Lapkin IY, Katz YI (1990) Geological events at the boundary of the carboniferous and Permian. Izvestiya, USSR Acad Sci Ser Geol 8:45–58

Lenoir J-L, Küster D, Liegeois J-R, Utke A, Haider A, Matheis G (1994) Origin and regional significance of late Precambrian and early Palaeozoic granitoids in the pan-African belt of Somalia. Geol Rundsch 83:624–641

Levin BW, Sasorova EV (2012) Seismotectonics and Earth tides. Russ J Pac Geol 6(1):70–77

Levin BV, Sasorova EV, Domanskii AV (2013) Properties of critical latitudes, rotation variations and Earth's seismicity. Bull Far East Branch Russ Acad Sci. Sect: Seismology 3:3–8. (in Russian)

Lian D, Yang J, Dilek Y, Wu W, Zhang Z, Xiong F, Liu F, Zhou W (2017) Deep mantle origin and ultra-reducing conditions in podiform chromitite: diamond, moissanite, and other unusual minerals in podiform chromitites from the Pozanti-Karsanti ophiolite, southern Turkey. Am Mineral 102:1101–1113

Logan JM (1977) Animal behaviour and earthquake prediction. Nature 265:404–405

Lucazeau F, Leroy S, Autin J, Bonneville A, Goutorbe B, Rolandone F, d'Acremont E, Watremez L, Düsünur D, Huchon P (2009) Post-rift volcanism and high heatflow at the ocean–continent transition of the Gulf of Aden. Terra Nova 21(4):285–292

Mahfoud RF (2002) Presence of diamond in the pyrope peridotite, Dreikeesh area, tartous province, NW Syria: a new theory on the origin of diamond. Microchem J 73(3):265–271

Martinez F, Cochran JR (1989) Geothermal measurements in the northern Red Sea: implications for lithospheric thermal structure anrifting. J Geophys Res 94(12):239–212, 265

Maus S, Sazonova T, Hemant K, Fairhead JD, Ravat D (2007) National Geophysical Data Center candidate for the world digital magnetic anomaly map. Geochem Geophys Geosyst 8(6):1–10. https://doi.org/10.1029/2007GC001643

McLusky S et al (2000) Global position system constraints on plate kinematics and dynamics in the eastern Mediterranean and Caucasus. J Geophys Res 105:5695–5719

Milesi JP, Frizon de Lamotte D, de Kock G, Toteu F (2010) Tectonic map of Africa, 1:10 000 000 scale. CCGM-CGMW, Paris

Moghadam HS, Corfu F, Stern RJ (2013) U-Pb zircon ages of Late Cretaceous Nain-Dehshir ophiolites, Central Iran. J Geol Soc Lond 170:175–184

Monismith SG, Genin A, Reidenbach NA, Yahel G, Koseff GR (2006) Thermally driven exchanges between a coral reef and the adjoining ocean. J Phys Ocean 36:1332–1347

Motavalli-Anbaran SH, Zeyen H, Brunet M-F, Anderstani VE (2011) Crustal and lithospheric structure of the Alborz Mountains, Iran, and surrounding areas from integrated geophysical modeling. Tectonics 30(TC5012):1–16

Mposkos ED, Kostopoulos DK (2001) Diamond, former coesite and supersilicic garnet in metasedimentary rocks from the Greek Rhodope: a new ultrahigh-pressure metamorphic province established. Earth Plan Sci Lett 192:497–506

Muluneh AA, Cuffaro M, Doglioni C (2014) Left-lateral transtension along the Ethiopian Rift and constrains on the mantle-reference plate motions. Tectonophysics 632:21–31

Muttoni G, Kent DV, Garzanti E, Brack P, Abrahamsen N, Gaetani M (2003) Early Permian Pangea 'B' to Late Permian Pangea 'A'. Earth Planet Sci Lett 215:379–394

Muttoni G, Gaetani M, Kent DV, Sciunnach D, Angiolini L, Berra F et al (2009) Opening of the Neo-Tethys Ocean and the Pangea B to Pangea A transformation during the Permian. GeoArabia 14(4):17–48

Neumeyer J, Barthelmes F, Dierks O, Flechtner F, Harnisch M, Harnisch G, Hinderer J, Imanishi Y, Kroner C, Meurers B, Petrovic S, Reigber C, Schmidt R, Schwintzer P, Sun H-P, Virtanen H (2006) Combination of temporal gravity variations resulting from superconducting gravimeter (SG) recordings, GRACE satellite observations and global hydrology models. J Geodesy 79:573–585

Nikonov AA (1992) Abnormal animal behavior as a precursor of the 7 December 1988 Spitak, Armenia, Earthquake. Nat Hazards 6:1–10

Nyblade AA (2011) The upper-mantle low-velocity anomaly beneath Ethiopia, Kenya, and Tanzania: constraints on the origin of the African superswell in eastern Africa and plate versus plume models of mantle dynamics. In Beccaluva L, Bianchini G, Wilson M (eds) Volcanism

and Evolution of the African Lithosphere, The Geological Society of America, Special paper 478, pp 1–14

Okay C, Toksoy-Köksal F, Öztüfeksi-Önal A, Aktağ A (2016) Depleted to refertilized mantle peridotites hosting chromitites within the Tunceli ophiolite, eastern Anatolia (Turkey): insights on the back arc origin. Ofioliti 41(1):1–20

Park Y, Nyblade AA, Rodgers AJ, Al-Amri A (2008) S wave velocity structure of the Arabian Shield upper mantle from Rayleigh wave tomography. Geochem Geophys Geosyst 9(7):1–15

Pasyanos ME, Nyblade AN (2007) A top to bottom lithospheric study of Africa and Arabia. Tectonophysics 444:27–44

Pollack HN, Hurter SJ, Johnson JR (1993) Heat flow from the Earth's interior: analysis of the global data set. Rev Geophys 31:267–280

Pollastro RM (2003) Total petroleum systems of the Paleozoic and Jurassic, Greater Ghawar uplift and adjoining provinces of Central Saudi Arabia and Northern Arabian-Persian Gulf. US Geol Surv Bull 2202-H:1–75

Reilinger R, McClusky S (2011) Nubia-Arabia-Eurasia plate motions and the dynamics of Mediterranean and Middle East tectonics. Geophys J Int 186:971–979

Reilinger RE, McClusky S, Vernant P, Lawrence S, Ergintav S, Cakmak R, Ozener H, Kadirov F, Guliev I, Stepanyan R, Nadariya M, Hahubia G, Mahmoud S, Sakr K, ArRajehi A, Paradissis D, Al-Aydrus A, Prilepin M, Guseva T, Evren E, Dmitrotsa A, Filikov SV, Gomez F, Al-Ghazzi R, Karam G (2006) GPS constraints on continental deformation in the Africa-Arabia-Eurasia continental collision zone and implications for the dynamics of plate interactions. J Geophys Res BO5411:1–26. https://doi.org/10.1029/2005JB004051

Reilly M (2009) Lunar cycle affects cyclone strength. ABC News, Mar 9

Riguzzi F, Panza G, Varga P, Doglioni C (2010) Can Earth's rotation and tidal despinning drive plate tectonics? Tectonophysics 484:60–73

Robertson AHF (1998) Mesozoic–Tertiary tectonic evolution of the Easternmost Mediterranean area: integration of marine and land evidence. In: Robertson AHF, Emeis KC, Richter C, Camerlenghi A (eds) Proc Ocean Drill Program Sci Results 160: 723–782

Robertson A (2004) Development of concepts concerning the genesis and emplacement of Tethyan ophiolites in the Eastern Mediterranean and Oman regions. Tectonophysics 66:331–387

Robertson AHF, Clift PD, Degnan PJ, Jones G (1991) Palaeogeographic and palaeotectonic evolution of the Eastern Mediterranean Neotethys. Palaeogeogr Palaeoclimatol Palaeoecol 87:289–343

Rolandone F, Lucazeau F, Leroy S, Mareschal J-C, Jorand R, Goutorbe B, Bouquerel H (2013) New heat flow measurements in Oman and the thermal state of the Arabian Shield and Platform. Tectonophysics 589:77–89

Roure F, Casero P, Addoum B (2012) Alpine inversion of the North African margin and delamination of its continental lithosphere. Tectonics 31(TC3006):1–28. https://doi.org/10.1029/2011TC002989

Said R (ed) (1990) The geology of Egypt. AA Balkema/Rotterdam/Brookfield

Sandwell DT, Smith WHF (2009) Global marine gravity from retracked Geosat and ERS-1 altimetry: ridge segmentation versus spreading rate. J Geophys Res 114(B01411):1–18

Sandwell DT, Garcia E, Soofi K, Wessel P, Smith WHF (2013) Toward 1 mGal global marine gravity from CryoSat-2, Envisat, and Jason-1. Lead Edge 32(8):892–899

Scafetta N (2010) Empirical evidence for a celestial origin of the climate oscillations and its implications. J Atmos and Sol Terr Phys 72:951–970

Sclater JG, Jaupart C, Galson D (1980) The heat flow through oceanic and continental crust and the heat loss of the Earth. Rev Geophys Space Phys 18(1):269–311

Scotese CR (2009) Late Proterozoic plate tectonics and palaeogeography: a tale of two supercontinents, Rodinia and Pannotia. Geol Soc Lond, Spec Publ 326:57–83

Segev A (2009) 40Ar/39Ar and K-Ar geochronology of Berriasian-Hauterivian and Cenomanian tectonomagnetic events in northern Israel: implications for regional stratigraphy. Cretac Res 30:810–828

Shatsky NS, Belyaevsky NA, Bogdanov AA, Muratov ME (1956) Tectonic map of the USSR and adjacent countries, scale 1: 5000000. Geosgeolizdat, Moscow

Sheldrake R (2005) Listen to the animals: why did so many animals escape December's tsunami? Ecologist 3:1–2

Stacy JS, Doe BR, Roberts RJ, Delevaux MH, Gramlich JW (1980) A lead isotope study of mineralization in the Saudi Arabian shield. Contrib Mineral Petrol 74:175–188

Stampfli GM, Borel GD (2002) A plate tectonic model for the Paleozoic and Mesozoic constrained by dynamic plate boundaries and restored synthetic oceanic isochrones. Earth Planet Sci Lett 196:17–33

Stampfli GM, Hochard C, Vérard C, Wilhem C, von Raumer J (2013) The formation of Pangea. Tectonophysics 593:1–19

Stamps DS, Iaffaldano G, Calais E (2014) Role of mantle flow in Nubia-Somalia plate divergence. Geophys Res Lett 42:290–296. https://doi.org/10.1002/2014GL062515

Stern RJ, Johnson P (2010) Continental lithosphere of the Arabian plate: a geologic, petrologic, and geophysical synthesis. Earth Sci Rev 101:29–67

Stern RJ, Johnson PR, Kroner A, Yibas B (2004) Neoproterozoic ophiolites of the Arabian-Nubian Shield. Dev Precambrian Geol 13:95–128

Suetsugu D, Isse T, Tanaka S, Obayashi M, Shiobara H, Sugioka H, Kanazawa T, Fukao Y, Barruol G, Reymond D (2009) South Pacific mantle plumes imaged by seismic observation on islands and seafloor. Geochem Geophys Geosyst 10:1–18

Tainton KM, Seggie AM, Bayly BA, Tomlinson I, Quadling KE (1999) Garnet thermobarometry: implication for mantle heat flow within the Tanzanian craton. In: Proceedings of the VIIth international Kimberlite Confreference. Red Roof Publishing CC, Cape Town, pp 852–860

Tunini L, Jimenez-Munt I, Fernandes M, Verges J, Villasenor A (2015) Lithospheric mantle heterogeneities beneath the Zagros Mountains and the Iranian Plateau: a petrological-geophysical study. Geophys J Int 200:596–614

Usoskin IG (2008) A history of solar activity over Millennia. Living Rev Sol Phys 5(3). http://www.livingreviews.org/lrsp-2008-3

Van der Meer DG, van Hinsbergen DJJ, Spakman W (2018) Atlas of the underworld: slab remnants in the mantle, their sinking history, and a new outlook on lower mantle viscosity. Tectonophysics 723:309–448

Verges J, Saura E, Casciello E, Fernandez M, Villasenor A, Jimenez-Munt I, Garsia-Castellanos D (2011) Crustal-scale cross-sections across the NW Zagros belt: implications for the Arabian margin reconstruction. Geol Mag:1–23. https://doi.org/10.1017/S0016756811000331

Véronnet A (1912) Rotation de l'Ellipsoide Hétérogène et Figure Exacte de la Terre. J Math Pures Appl 6(8):331–463

Verzhbitsky EV (1996) Geothermal regime and tectonics of marine areas bottom along the alpine-Himalayan Belt. Nauka, Moscow. (in Russian)

Wdowinski S, Bock Y, Baer G, Prawirodirdjo L, Bechor L, Naaman S, Knafo R, Forrai Y, Melzer Y (2004) GPS measurements of current crustal movements along the Dead Sea Fault. J Geophys Res 109(B05403):1–16. https://doi.org/10.1029/2003JB002640

Weissbrod T (2005) The Paleozoic in Israel and environs. In: Hall JK, Krasheninnikov VA, Hirsch F, Benjamini C, Flexer A (eds) Geological framework of the Levant, vol 2. The Levantine Basin and Israel, Jerusalem, pp 283–315

Wen L, Helmberger DV (1998) Ultra-low velocity zones near the core-mantle boundary from broadband PKP precursors. Science 279:1701–1703

Wiltschko R, Wiltschko W (2014) Sensing magnetic directions in birds: radical rair processes involving cryptochrome. Biosensors 4:221–242

Wuebbles DJ, Kunkel K, Wenher M, Zobel Z (2014) Severe weather in Unites States under a changing climate, 2014. EOS AGU Trans 95(18):149, 156

Yakobson AN (1997) Velocity of shear seismic waves in the Southern Caspian lithosphere. Dokl Russ Acad Sci 302(2):258–260

Yamasaki T, Stephenson R (2011) Back-arc rifting initiated with a hot and wet continental lithosphere. Earth Planet Sci Lett 302(1–2):172–184

Yaroshevich MI (2011) On some signatures of gravity anomaly influence to tropical cyclones of the north-west part of the Pacific Ocean. Dokl Russ Acad Sci 437(4):548–552